Received: 29 May 2020 | Revised: 9 December 2020 | Accepted: 10 December 2020

DOI: 10.1002/esp.5055

RESEARCH ARTICLE

ESPL WILEY

Geometry of obstacle marks at instream boulders—integration of laboratory investigations and field observations

Oliver Schlömer[1] | **Paul E. Grams**[2] | **Daniel Buscombe**[3,4] | **Jürgen Herget**[1]

[1]Department of Geography, University of Bonn, Bonn, Germany

[2]U.S. Geological Survey, Southwest Biological Science Center, Grand Canyon Monitoring and Research Center, Flagstaff, Arizona, USA

[3]School of Earth and Sustainability, Northern Arizona University, Flagstaff, Arizona, USA

[4]Marda Science, Flagstaff, Arizona, USA

Correspondence
Oliver Schlömer, Department of Geography, University of Bonn, Meckenheimer Allee 166, 53115 Bonn, Germany.
Email: schloem@uni-bonn.de

Abstract

Obstacle marks are instream bedforms, typically composed of an upstream frontal scour hole and a downstream sediment accumulation in the vicinity of an obstacle. Local scouring at infrastructure (e.g. bridge piers) is a well-studied phenomenon in hydraulic engineering, while less attention is given to the time-dependent evolution of frontal scour holes at instream boulders and their geometric relations (depth to width, and length ratio). Furthermore, a comparison between laboratory studies and field observations is rare. Therefore, the morphodynamic importance of such scour features to fluvial sediment transport and morphological change is largely unknown. In this study, obstacle marks at boulder-like obstructions were physically modelled in 30 unscaled process-focused flume experiments (runtime per experiment ≥ 5760 min) at a range of flows (subcritical, clear-water conditions, emergent and submerged water levels) and boundary conditions designed to represent the field setting (i.e. obstacle tilting, and limited thickness of the alluvial layer). Additionally, geometries of scour holes at 90 *in-situ* boulders (diameter ≥ 1 m) located in a 50-km segment of the Colorado River in Marble Canyon (AZ) were measured from a 1 m-resolution digital elevation model. Flume experiments reveal similar evolution of local scouring, irrespective of hydraulic conditions, controlled by the scour incision, whereas the thickness of the alluvial layer and obstacle tilting into the evolving frontal scour hole limit incision. Three temporal evolution phases—(1) rapid incision, (2) decreasing incision, and (3) scour widening—are identified based on statistical analysis of spatiotemporal bed elevation time series. A quantitative model is presented that mechanistically predicts enlargement in local scour length and width based on (1) scour depth, (2) the inclination of scour slopes, and (3) the planform area of the frontal scour hole bottom. The comparison of field observations and laboratory results demonstrates scale invariance of geometry, which implies similitude of processes and form rather than equifinality.

KEYWORDS
boulders, local scour, obstacle marks, processes and form, similitude

1 | INTRODUCTION

Obstacle marks are bed features related to topographic obstructions exposed to a current (Hargitai, 2014; Karcz, 1968; Richardson, 1968). Typically, obstacle marks are composed of an upstream crescentic frontal scour hole that laterally surrounds the obstacle in the downstream direction, and a dune-like sediment accumulation in the downstream wake of the obstruction, termed 'sediment ridge' (Oliveto & Hager, 2014). Obstacle marks emerge due to three-dimensional flow structures and turbulence in the vicinity of an obstacle, even when the threshold velocity for general sediment movement is not exceeded (Euler & Herget, 2012). Obstacles may be large

natural bed elements such as solitary boulders or deadwood with a diameter greater than the mean diameter of the surrounding alluvium (Judd & Peterson, 1969; Laronne et al., 2001; Lisle, 1981; Thompson, 2008), or instream infrastructure (i.e. bridge piers, spur dikes) (Breusers & Raudkivi, 1991; Hoffmans & Verheij, 1997; Melville & Coleman, 2000). Thus, the flow structures around instream obstacles and the formation of obstacle marks are relevant to various scientific disciplines in Earth science and hydraulic engineering.

In geomorphology and sedimentology, depositional patterns around isolated small boulders or cobbles in gravel-bed rivers are well documented as particle clusters (Carling & Reader, 1982; Cin, 1968; Papanicolaou et al., 2018; Storm & Papanicolaou, 2007). However, in contrast to an obstacle mark, local scouring at the stoss side of particle clusters is inhibited because individual grains are large relative to the cluster and dissipate energy (Lee & Sturm, 2009). Instead of initiating erosion, particle clusters tend to trap incoming sediment that is transported as bedload sheets or in suspension, either on its stoss side or its wake, depending on the submergence ratio (ratio of approaching flow depth to size of the obstacle) (Ghilardi et al., 2014; Papanicolaou et al., 2011, 2012) and the turbulent flow structure (Lawless & Robert, 2001). Deposits of finer material form frequently in the low-energy wake of large bed obstructions, presumably during waning flows (Carling & Reader, 1982; Thompson, 2008).

Obstacle mark formation at boulder-like obstructions has been described in relatively few empirical laboratory studies (Boyer & Roy, 1991; Euler et al., 2017; Fisher & Klingman, 1984; Shamloo et al., 2001). The submergence ratio is a particularly important boundary condition, as boulder-like instream obstructions are affected by different water levels. During lower flows, the obstacle might be emergent (some portion of the obstacle protrudes above the water surface) and the flow is affected by localized flow structures (e.g. hydraulic jumps) as it becomes a function of the Froude number. Meanwhile at higher flow, the obstacle occupies only the lower portion of the flow depth and is submerged, while the flow is subcritical (Boyer & Roy, 1991; Papanicolaou et al., 2010; Shamloo et al., 2001).

Moreover, obstacle mark formation at boulder-like instream obstructions in the field is influenced by specific boundary conditions that limit scouring (Schlömer et al., 2020). For instance, scour incision at a solitary instream boulder causes the boulder to tilt into the frontal scour hole once a critical depth is crossed, resulting in self-burial of the obstacle (Euler et al., 2017). Consequently, this process changes the boulder's exposure to flow and alters the scouring processes (Rennie et al., 2017). In contrast, the alluvial layer in which the boulder is embedded might be depth-limited, so that only a thin alluvial cover is present over bedrock (Hodge et al., 2011), or an armour layer is developed in the scour hole due to non-uniformity of alluvial material. In both cases, ongoing scour incision is restricted due to these morphodynamic feedback mechanisms.

In summary, these specific limiting boundary conditions that control local scour around boulders in the field have been insufficiently investigated via systematic laboratory studies, while integration between laboratory results on obstacle mark geometry with field evidence has rarely been carried out. Improved understanding of the geometry of obstacle marks is needed to (a) refine existing procedures to estimate the magnitude of past flood events (Herget et al., 2013), and (b) estimate the spatial extent of countermeasures for local scour protection at technical infrastructure. Consequently, the aims of the present contribution are:

i. To analyse the processes of enlargement and the resulting geometry of evolving frontal scour holes at boulder-like obstructions under various hydraulic conditions via a systematic laboratory flume study.
ii. To evaluate local scouring at boulder-like obstructions in consideration of limiting boundary conditions of obstacle mobility and in the presence of a depth-limited alluvial layer via a systematic laboratory flume study.
iii. To investigate possible scale invariance and geometric similitude of frontal scour holes by comparing laboratory results to *in-situ* obstacle marks at boulders in the Colorado River documented in a digital elevation model (DEM) derived from bathymetric mapping in Marble Canyon (Arizona) (Kaplinski et al., 2017a).

1.1 | Geometry of obstacle marks

The morphology (i.e. frontal scour hole and downstream sediment ridge) is characterized by certain morphometric variables, including scour hole depth at the obstacle front (d_s), measured from the undisturbed upstream bed; scour hole frontal length (l_s) in the plane of symmetry to the incoming flow, measured from the obstacle frontal face to the upstream edge of the scour hole; and scour hole frontal width (w_s), measured perpendicular to the direction of incoming flow from the lateral edges of the scour hole at the obstacle frontal face (Figure 1a). A corresponding definition can be applied to the sediment ridge, including sediment ridge height (h_r), sediment ridge width (w_r), and sediment ridge length (l_r), measured from the downstream end of the obstruction (Euler & Herget, 2012).

The applied engineering practice focuses on physical modelling to determine predictive equations for equilibrium d_s, defined as the maximum depth of the frontal scour hole that is likely after prolonged exposure to steady flow. Equilibrium d_s is used as a design parameter for foundation depth (Pizarro et al., 2020; Simarro et al., 2011), or as a proxy in risk assessment procedures (Tubaldi et al., 2017). The evolution of d_s is an asymptotic process in time (Kothyari et al., 1992; Lu et al., 2011; Mohammadpour et al., 2017; Oliveto & Hager, 2002, 2005). From laboratory data at clear-water conditions (flow velocity < threshold velocity for sediment mobilization), it is well established that 80% of equilibrium d_s is developed within only 5–40% of the time to equilibrium that is obtained after several days, mainly depending on flow velocity and grain size (Melville & Chiew, 1999).

Although recent studies have examined the evolution of scour-hole geometry for different types of obstacles and sediment sizes, by utilizing a range of measurement methods (Bouratsis et al., 2013, 2017; Diab et al., 2010; Link et al., 2008; Poggi & Kudryavtseva, 2019; Rogers et al., 2020; Sarkar et al., 2015), these studies have focused on d_s, while ignoring w_s and l_s. Nevertheless, there is general agreement that the geometry of frontal scour holes can be approximated as an inverted frustum cone with an elliptical shape in plan view ($l_s < w_s$) (Figure 1a) (Mia & Nago, 2003), whereas the longitudinal shape (i.e. in the flow direction) is quite symmetrical (Schalko et al., 2019; Schlömer, 2020). However, considering a longitudinal profile from the obstacle frontal face to the upstream edge of the scour hole

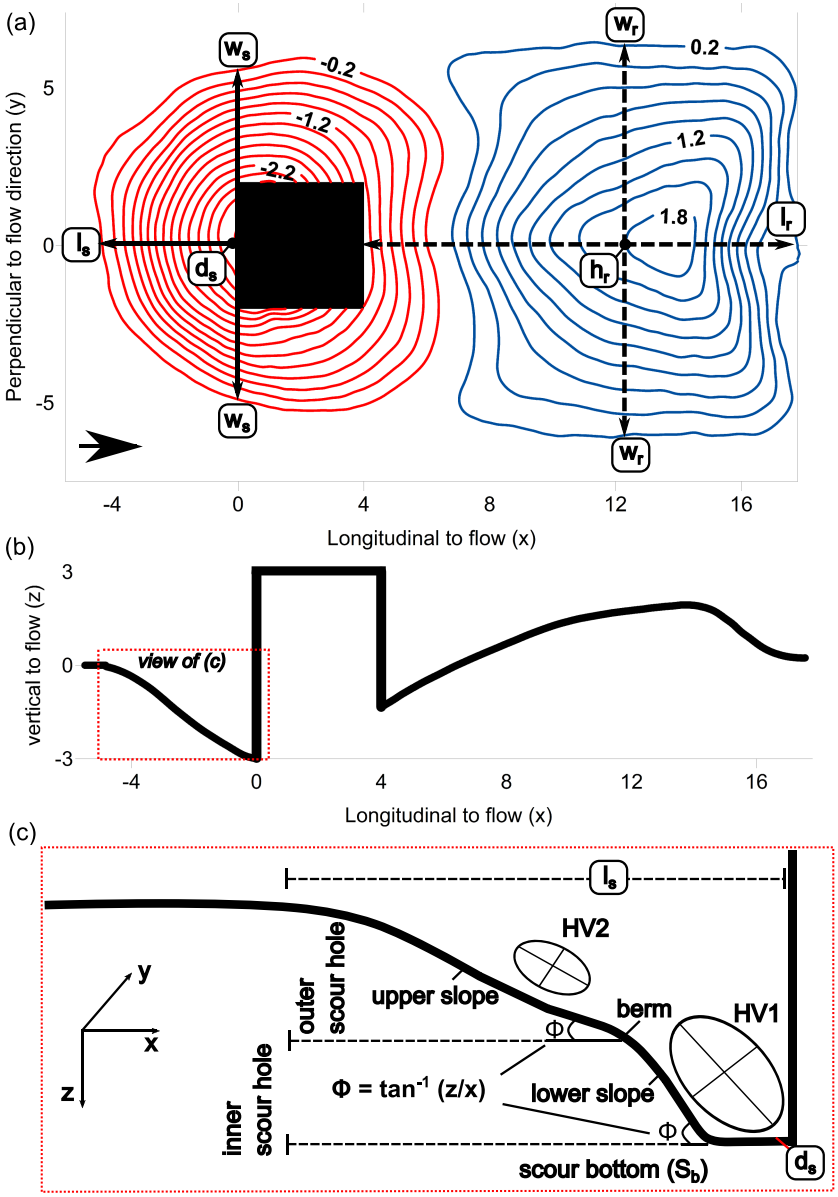

FIGURE 1 (a) Plan view of a typical obstacle mark at a cuboid obstacle generated in a flume defining characteristic morphometric variables of frontal scour hole (red isolines) and sediment ridge (blue isolines) (scale is in centimetres, large arrow indicates direction of flow). (b) Longitudinal cross-section in the plane of symmetry. (c) Upstream cross-sectional profile of the frontal scour hole indicating internal differentiation and positions of primary horseshoe vortex (HV1) in back-flow mode, and secondary horseshoe vortex (HV2) (not to scale) [Colour figure can be viewed at wileyonlinelibrary.com]

at equilibrium condition, different segments are distinguishable. These segments consist of: (1) a flat semi-circular scour hole bottom (S_b) that is closely attached to the obstacle base with radius < l_s; (2) an inner frontal scour hole (lower slope) that is characterized by an inclination ≥ critical angle of repose (Φ_{crit}); and (3) an outer frontal scour hole (upper slope) that is characterized by an inclination ≤ Φ_{crit} (Figures 1b and c). The transition between both slopes is marked by a knickpoint (berm) in the cross-sectional profile.

1.2 | Morphodynamic processes at instream obstacles

Obstacle marks originate from deformations of the approaching flow in the vicinity of the obstacle that result in the following processes: (1) contraction of streamlines lateral to the obstacle, causing higher flow velocities; (2) a vertical jet-like downflow towards the bed that emerges due to the pressure gradient at the obstacle frontal face; (3) formation of a turbulent vortex structure at the obstacle base, resulting from the deflection of the downflow against the main flow direction—because the vortex structure wraps laterally past the sides of the obstacle in the downstream direction, it is commonly referred to as a horseshoe vortex (HV); and (4) a decelerated region of flow in the wake of the obstruction, including a wake vortex system of detached shear layers with a vertical axis of rotation (Bauri & Sarkar, 2016; Dargahi, 1990; Escauriaza & Sotiropoulos, 2011a; Hunt et al., 1978; Launay et al., 2017; Papanicolaou & Tsakiris, 2017; Pattenden et al., 2005; Schlömer et al., 2020; Shamloo et al., 2001; Sumner, 2013) (Figure 2).

Processes (1) to (3) amplify the bed shear stress above the critical bed shear for sediment mobilization, inducing local scouring in front and lateral to the obstacle in non-cohesive and cohesive sediment (Allen, 1982; Sonia Devi & Barbhuiya, 2017).

The enlargement of the frontal scour hole and its geometry are closely related to the HV as the main driver of sediment mobilization (Dargahi, 1989; Li et al., 2018; Radice & Tran, 2012; Radice et al., 2009). The HV actually consists of several interacting and unsteady vortices (Chen et al., 2017; Escauriaza & Sotiropoulos, 2011b; Kirkil & Constantinescu, 2010; Kirkil et al., 2008). The largest and most stable vortex is denoted as the primary horseshoe vortex (HV1) and is

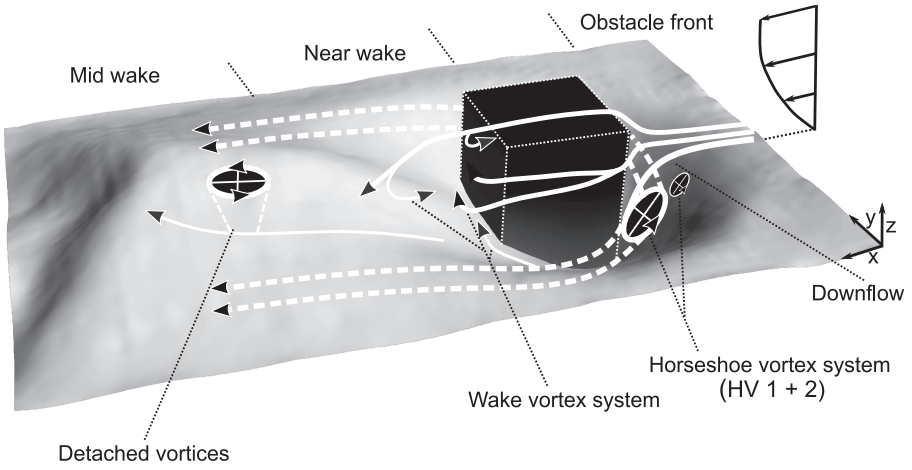

FIGURE 2 Schematic flow field in the vicinity of a submerged cuboid obstacle. Flow direction from right to left (modified after Schlömer et al., 2020)

located close to the obstacle base. During incision, HV1 sinks into the frontal scour hole and extends down to S_b, where it promotes sediment mobilization by saltation and rolling (Chen et al., 2019; Dargahi, 1990; Dey & Raikar, 2007). Upstream of HV1, a smaller and less coherent vortex (HV2) is located within the outer region of the frontal scour hole (Figures 1c and 2). HV2 can completely lose coherence, while HV1 exhibits aperiodic bimodal oscillations that cause changes in the position and shape of the vortex core, from circular (zero-flow mode) and closely aligned to the obstacle, to elliptical (back-flow mode), where the core is situated away from the obstacle (Kirkil & Constantinescu, 2015; Paik et al., 2007). In back-flow mode, the vertical extent of HV1 coincides with the knickpoint in the slopes, differentiating the outer and inner frontal scour hole (Muzzammil & Gangadhariah, 2003; Unger & Hager, 2007). Although the rotation of the HV generally stabilizes the lower slope at an angle greater than Φ_{crit} (Hoffmans, 1993), the aforementioned temporal oscillations (HV1) and occasional disappearance (HV2) destabilize the slopes and result in collapse characterized by gravitational movements into S_b. In shallow flow (flow depth <<< channel width) and emergent conditions at the obstacle, a surface standing wave at the junction between the upstream frontal face of the obstacle and the free surface is formed (Boyer & Roy, 1991; Shamloo et al., 2001). This bow wave can affect HV1 as the vortices have opposite direction of rotation (Gazi & Afzal, 2020). With decreasing flow depth, the bow wave dominates and HV1 is less capable of entraining sediment (Melville & Coleman, 2000). Schlömer et al. (2020) have documented that the dimensions of the frontal scour hole are reduced if submergence ratio ≤ 0.55.

1.3 | Boundary conditions of obstacle mark formation

The formation of marks at natural obstacles is impacted by different extrinsic and intrinsic environmental boundary conditions that comprise (1) flow conditions, (2) sediment characteristics, (3) properties of the obstacle, and (4) time. Recently, Schlömer et al. (2020) have proposed a functional relationship of scale-invariant parameters that control local scouring at solitary boulder-like obstructions located in a straight, moderately sloped channel and cohesionless alluvial sediment. The non-dimensional control parameters, derived on principles of the Buckingham Π theorem (e.g. Barenblatt, 2003), result in an expression for local scour incision d_s/L_o:

$$d_s/L_o = f(d_w/L_o, U_m/U_c, Re_o, L_o/B, Sh, Mb, L_o/D_{50}, \sigma_G, d_{sed}/L_o, t/t_e) \quad (1)$$

where d_w/L_o is the submergence ratio (d_w = flow depth [L] and L_o = effective obstacle size ${h_o}^{2/3}{w_o}^{1/3}$ [L], with h_o = obstacle height [L] and w_o = obstacle width [L], U_m/U_c is flow intensity (U_m = mean approach velocity [LT^{-1}] and U_c = critical mean approach velocity for entrainment of sediment [LT^{-1}]), Re_o is the obstacle Reynolds number ($U_m L_o/\nu$, with ν = kinematic viscosity of water [L^2T^{-1}]), L_o/B is the blockage ratio (with B = channel width [L]), Sh [–] is an indicator for the hydrodynamic shape of the obstacle, Mb [–] is an indicator for the mobility of boulder-like obstruction due to tilting into the local scour hole, L_o/D_{50} is the relative sediment coarseness (D_{50} = median diameter of the bed sediment [L]), σ_G is the sorting of sediment (${D_{84}/D_{16}}^{1/2}$ [–]), d_{sed}/L_o is the relative thickness of the alluvial layer (d_{sed} = thickness of the alluvial layer in which the obstacle is embedded [L]), and t/t_e is the time scale of local scouring.

Each term in Equation (1) is measurable or readily simulated with the current state-of-the-art technology for measuring or modelling three-dimensional flows and time-dependent riverbed elevation evolution.

1.4 | Obstacle marks at different spatial scales

Field evidence of obstacle marks has been described for a range of conditions, including overland flow at rock fragments (Jomaa et al., 2012; Poesen et al., 1994) and around solitary boulders in flash floods in ephemeral streams (Euler et al., 2017; Karcz, 1972). Among the largest measured obstacle marks (dimensions up to 10^2 m) are those associated with large boulders and bedrock hills, hypothesized to have formed during Quaternary megafloods (Baker & Bunker, 1985; Carling et al., 2002; Herget, 2005). The dominant morphology (cf. Figure 1a) is thereby consistent over a range of spatial scales.

Contrary to the dominant morphology, local scour holes in the wake of boulders located in high-gradient step-pool streams (e.g. Comiti et al., 2005) and rock sills (e.g. Pagliara & Palermo, 2008, 2018) are reported. This plunge pool scour occurs as a result of an

overtopping jet-stream motion that differs from the HV-induced morphodynamic processes.

Nevertheless, field measurements of frontal scour hole geometry are extremely limited. Although bridge pier scour is frequently monitored in the USA, only d_s is considered among candidate morphometric variables (Mueller & Wagner, 2005; USGS National Bridge Scour Database, 2020). To the authors' knowledge, only the study by Butch (1991, 1999) has measured *in-situ* frontal scour hole geometry (d_s and w_s according to the definition in Figure 1a) at 128 bridge piers. The analysis of field measurements of d_s is complicated, owing to the difficulty in connecting scour hole measurements with the formative flow conditions (e.g. Link et al., 2019; Pizarro et al., 2020), exacerbated by uncertainty in the maturity of d_s at the time of measurement (Sheppard et al., 2014). In general, laboratory estimates of d_s tend to overestimate the actual dimensions of d_s in the field (Johnson et al., 2015; Pizarro & Tubaldi, 2019).

2 | MATERIALS AND METHODS

2.1 | Facility for laboratory studies

Physical modelling was conducted in a 5 m long, 0.32 m wide, 0.27 m deep straight, rectangular flume with fixed slope (0.003 m m^{-1}) entirely filled with a layer of uniform (σ_G < 1.3) sand with median grain diameter (D_{50} = 0.75 mm). Φ_{crit} of the sediment when dry is ~33° (Dey, 2014). Discharge (Q) was controlled by a recirculating pump, while flow depth (d_w) was adjusted by a tail-gate at the downstream end of the flume to enable pseudo-uniform flow within the working section of the flume (~270 cm downstream of the inlet) (Hager & Hutter, 1984). The water surface profile was measured using an ultrasonic distance meter (Mic +25, Microsonic®, accuracy ±0.1 mm). The unscaled flume experiments are interpreted as a process-focused physical model (Baynes et al., 2018) that attempts to reproduce processes and resulting morphologies, but does not represent a specific natural prototype.

Two obstacles of identical size (L_o = 3 cm) but different shape (cube, $Sh \geq 0.8$ and sphere, $Sh \leq 0.6$) were used to mimic boulder-like obstructions (i.e. angular and rounded). The obstacles were placed in the working section of the flume in the plane of symmetry to minimize sidewall effects (Nakagawa & Nezu, 1993). Blockage ratio (L_o/B, with B = flume width) and relative sediment coarseness (L_o/D_{50}) were designed to satisfy critical thresholds for the onset of local scouring: $L_o/D_{50} > 8$ (Lee & Sturm, 2009) and $L_o/B < 0.6$ (Chou & Chao, 2000; Williams et al., 2019).

The flume was used for a total of 30 individual runs, comprised of three different experimental configurations (Figure 3a).

In series A, the obstacles were mounted to the flume bottom such that the entire obstacle (L_o = 3 cm) was above the initial bed (d_{sed} = 5.5 cm), and exposed to 10 different hydraulic conditions by variations in d_w/L_o (0.67–4) and U_m/U_c (0.49–0.81).

In series B, the obstacles were mounted to the flume bottom with L_o above the initial bed (d_{sed} = 2 cm) and exposed to hydraulic conditions of series A.

In series C, the obstacles were loosely placed on the bed with L_o above the initial bed (d_{sed} = 5.5 cm), but the obstacles were free to move and were exposed to hydraulic conditions of series A and B.

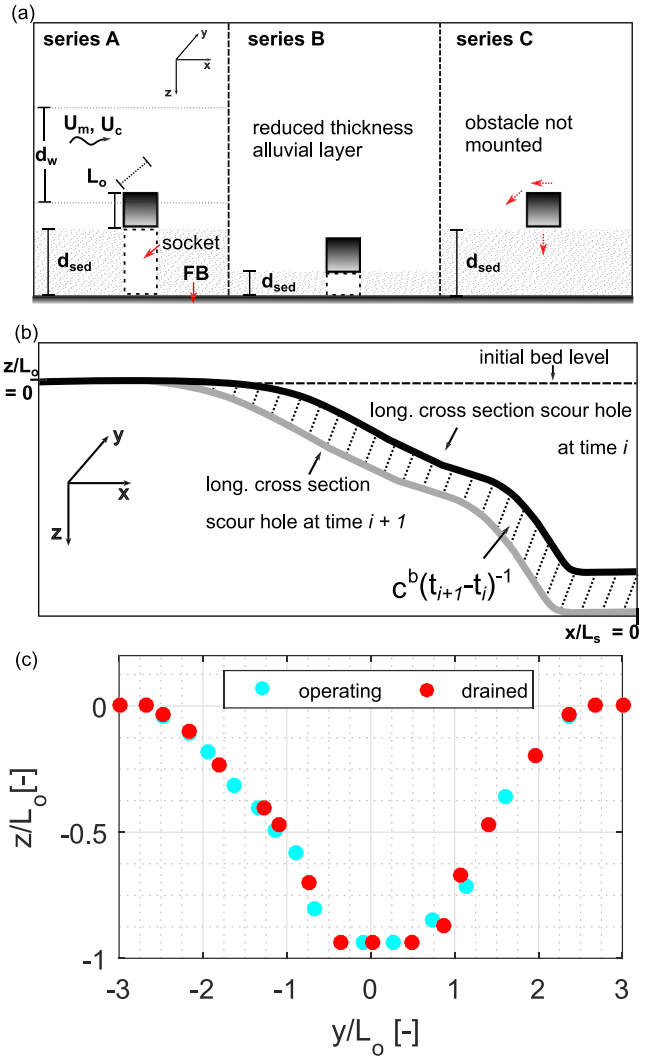

FIGURE 3 (a) Side view of experimental setups within the working section of the flume; FB = flume bottom. (b) Definition of subsequent cross-sections for the estimation of the sediment transport rate (q^b) exemplified for the upstream cross-section of the frontal scour hole in non-dimensional form. (c) Point measurements of upstream horizontal cross-section in non-dimensional form for run A6 displaying calibrated measurements while flume was operating (cyan) and drained (red) [Colour figure can be viewed at wileyonlinelibrary.com]

2.2 | Working hypotheses for experimental series

By neglecting constant boundary conditions of the experiments (L_o/B = 0.09, L_o/D_{50} = 40, σ_G < 1.3), scour depth incision can be functionally formulated as

$$d_s/L_o = f(d_w/L_o, U_m/U_c, Re_o, Sh, Mb, t/t_e) \quad (2)$$

By assuming shape similitude of the local scour hole, non-dimensional scour depth (d_s/L_o) in Equation (2) can be replaced by non-dimensional scour length (l_s/L_o) or non-dimensional scour width (w_s/L_o).

Furthermore, it is hypothesized that for given sediment size and obstacle size, l_s/L_o and w_s/L_o will scale with d_s/L_o, obstacle shape (Sh) and elapsed time of the experiments (t/t_e), and only indirectly with the actual flow conditions. The same hypothesis is required for the

methodology proposed by Chreties et al. (2008). Each experiment lasted 5760 min, which for given U_m/U_c and L_o/D_{50} is two to five times larger than the estimated time scale to attain equilibrium d_s proposed by Melville and Chiew (1999). The long-duration experiments were chosen, because no empirical values for equilibrium l_s and w_s are reported. Hence, t_e is interpreted as the absolute runtime of individual experiments.

The working hypothesis for series A is:

A. The dimensions of l_s/L_o and w_s/L_o in time are dependent on d_s/L_o and essentially unaffected by flow conditions.

Therefore, Equation (2) reduces to a form more amenable to empirical evaluation:

$$l_s/L_o, w_s/L_o = f(d_s/L_o, Sh, t/t_e) \quad (3)$$

In series B experiments, frontal scour hole incision into a depth-limited alluvial layer was evaluated by reducing d_{sed} such that $d_{sed}/L_o < 1$ limits scour incision.

The working hypothesis for series B is:

B. In the presence of a depth-limited alluvial layer, the time evolution of d_s/L_o depends solely on d_{sed}/L_o.

Thus, Equation (2) reduces to

$$d_s/L_o = f(d_{sed}/L_o, Sh, t/t_e) \quad (4)$$

The working hypothesis for series C is:

C. Obstacle tilting into the frontal scour hole alters the process dynamics of scour incision in time and impacts the geometric relations (i.e. d_s/l_s, d_s/w_s). Thus, Equation (2) reduces to

$$d_s/L_o, l_s/L_o, w_s/L_o = f(Mb, Sh, t/t_e) \quad (5)$$

TABLE 1 Non-dimensional hydraulic boundary conditions of all experimental series

Run	Type	d_w/L_o	U_m/U_c[†]	Fr
A1	C	0.67	0.67	0.37
A2	C	1	0.62	0.3
A3	C	2	0.55	0.22
A4	C	4	0.49	0.15
A5	C	0.67	0.81	0.45
A6	C	1	0.75	0.37
A7	C	2	0.66	0.26
A8	C	4	0.6	0.18
A9	C	2	0.79	0.31
A10	C	4	0.71	0.22
A11	S	0.67	0.67	0.37
A12	S	1	0.62	0.3
A13	S	2	0.55	0.22
A14	S	4	0.49	0.15
A15	S	0.67	0.81	0.45
A16	S	1	0.75	0.37
A17	S	2	0.66	0.26
A18	S	4	0.6	0.18
A19	S	2	0.79	0.31
A20	S	4	0.71	0.22
B1	C	4	0.6	0.18
B2	C	2	0.66	0.26
B3	C	1	0.75	0.37
B4	S	4	0.6	0.18
B5	S	2	0.66	0.26
B6	S	1	0.75	0.37
C1	C	2	0.66	0.26
C2	C	2	0.79	0.31
C3	S	2	0.66	0.26
C4	S	2	0.79	0.31

C = cube, S = sphere.
[†]U_c = 5.75 log (5.53 d_w/D_{50}) u_c^*, with u_c^* = 0.015+0.0125 $D_{50}^{1.4}$ (0.1 < D_{50} < 1 mm).

2.3 | Hydraulic boundary conditions of experimental series

Steady and subcritical flow conditions at clear-water conditions (U_m/U_c < 1) were designed by choosing different values of U_m (16.5, 20 and 24 cm s^{-1}) and different flow depths (2, 3, 6 and 12 cm) to mimic emergent ($d_w < L_o$) and fully submerged conditions ($d_w >> L_o$) at the obstacles. For given D_{50} and different values of d_w, U_c was computed by a procedure given in Melville and Coleman (2000) (see annotations to Table 1).

2.4 | Experimental procedure

The dimensions of d_s, l_s and w_s were measured with two LED distance meters (Welotec® OWRB series, accuracy ±0.5 mm), measuring x- and y-coordinates in a local Cartesian coordinate system, with x = longitudinal, streamwise direction and y = horizontal, perpendicular to streamwise direction; and a laser distance meter (Baumer Electric® ODAM S14C, accuracy ±1.5 mm) measuring the vertical coordinate (z). The sensors were mounted on a traversing system on top of the flume operating in the x/y plane. The elevation of the initial flat bed in front of the obstacle was used as reference (i.e. $x_0/y_0/z_0$ = 0/0/0). For individual runs, measurements of d_s, l_s and w_s were sampled at t = 1, 2.5, 5, 7.5, 10, 12.5, 15, 17 and 20 min (start of the experiment at t = 0 min). Irrespective of time, the spatial extent of l_s and w_s was obvious and determined by z_0 < 0. For $t \leq$ 480 min, the measuring interval was relaxed to 10 min. For t > 480 min, measurements were randomly sampled, while for $t \geq$ 1000 min, morphometric variables were measured only once in 1440 min up to the total runtime of experiments (5760 min).

The geometry of the frontal scour hole was measured by two-dimensional cross-sectional profiles in the longitudinal (i.e. streamwise) and horizontal (i.e. perpendicular to streamwise)

directions according to the definition in Figure 1a (solid lines). Profiles were surveyed at t = 30, 60, 120, 240 and 480 min, while for t > 480 min profiles were randomly sampled once in 1440 min.

Measurements of morphometric variables and profiles are interpreted as quasi-dynamic observations, because they were measured while water was flowing (Rogers et al., 2020). A systematic error was present for measurements of the z-coordinate due to refraction of the laser beam within the water column. Therefore, a simple calibration (i.e. compensation for the travel time of light in water) was applied to the raw data. The compensation procedure yielded sufficiently accurate results when compared to measurements at drained condition with the same measurement system (Figure 3c). The test reproducibility was successfully evaluated for repetitions of runs A6, A9, A10, A16 and A17, producing an average standard error of $d_s \sim 3\%$, $l_s \sim 6\%$ and $w_s \sim 4\%$.

Considering two consecutive frontal scour profiles, the volumetric bed load transport rate (q^b [L^2T^{-1}]) out of the frontal scour in absence of sediment suspension was estimated by calculating the line integral (Figure 3b)

$$q^b(l_{sP} \vee w_{sP}, t) \approx c^b / t(i+1) - t(i) \quad (6)$$

with l_{sP} = longitudinal scour hole profile, w_{sP} = horizontal scour hole profile, c^b = depth-integrated frontal scour hole area, i = 1, …, N, with N the total number of measured profiles in time.

For the subsequent analysis, q^b in Equation (6) is replaced by the dimensionless bed load q^* [−]:

$$q* = q^b / \left((\rho_s/\rho - 1) g {D_{50}}^3 \right)^{1/2} \quad (7)$$

with ρ = water density [ML^{-3}] and ρ_s = sediment density [ML^{-3}].

For comparison, frontal scour hole profiles were scaled with the corresponding dimensions of d_s, l_s and w_s, in order to preserve collinearity of distances and angles (i.e. three or more points initially lying on a line still lie on a line after the transformation) (Tregnaghi et al., 2007).

2.5 | Field data

Field observations of obstacle marks at boulders were derived from a DEM of a 50-km segment of the Colorado River within Grand Canyon National Park (Figure 4). The DEM is the result of a field survey in May 2009 in which bathymetric (multi-beam and single-beam sonar), topographic (ground-based total-station surveys) and grain size data were surveyed in order to monitor the status and trends of sediment storage along the Colorado River (Grams et al., 2019; Kaplinski et al., 2017a). Surveys were not conducted in rapids and riffles (Kaplinski et al., 2017a), thus all obstacles and associated obstacle marks were submerged ($d_w > L_o$) during the survey. The DEM has 1 m resolution and is projected to Arizona Central Zone of the State Plane Coordinate System of 1983, while elevations are ellipsoid heights (i.e. relative to the NAD83 ellipse). Bed-sediment maps were constructed using the methods reported in Buscombe et al. (2014a,b, 2017) at 0.25 m resolution and classify sediment into the Wentworth classes of sand, gravel and undifferentiated cobble/boulder/bedrock. The study area is located in Lower Marble Canyon (Figure 4) between river mile (RM) 30 and 61, which is the distance downstream from Lees Ferry, Arizona (RM 0) along a digitized channel centreline (Grams et al., 2019). The upstream extent of the study area is located 75 km downstream from Glen Canyon Dam. The river flows in a bedrock-walled canyon with an average channel width of 100 m at low discharge (∼225 m^3 s^{-1}), except for segments where tributary debris fans constrict flow and create rapids (channel width < 30 m) (Grams et al., 2019). Downstream of the debris fans, lateral flow recirculation zones (eddies) form (channel width up to 150 m) (Grams et al., 2013; Hazel et al., 2006). The river bed is dominated by sand and gravel, and the Paria River (Figure 4) is the primary source of fine sediments (Buscombe et al., 2017). River discharge is controlled by dam releases for hydroelectric power generation, which varies irregularly (monthly and seasonally) and regularly (a daily fluctuation with a constant period). During May 2009, the mean discharge at Lees Ferry was relatively low (∼270 m^3 s^{-1}) (Grams et al., 2013), and flow variability around the time of field measurements was likely minimal while the total sediment load was comparatively small at that time.

The DEM was processed using GIS to measure dimensions of the obstacle (h_o, w_o) and the dimensions of d_s, l_s, w_s within the resolution of the DEM (i.e. ≥1 m). Profiles of the frontal scour hole (cf. Figure 1a) were drawn equivalent to the processing of the laboratory data. The profiles began at the lowest bed elevation at the obstacle frontal face, or at the lowest elevation at the lateral edges of the obstacle (i.e. d_s), and ended where the bed elevation no longer increases with distance from the obstacle frontal face (Butch, 1999). The elevation of the surrounding bed was therefore considered to be z = 0. The profiles were scaled and post-processed to estimate local minima (i.e. d_s) and maxima (i.e. h_o and w_o).

3 | RESULTS

3.1 | Scour hole evolution at laboratory scale

In runs A1 to A10, two small depressions developed immediately at the lateral edges of the obstruction and merged rapidly to form a frontal scour hole ($t/t_e \approx 0.0001$–0.0004). The eroded material was deposited downstream in the wake of the obstruction as a sediment ridge with orientation parallel to the flow direction, forming the typical obstacle mark morphology. Subsequently, the frontal scour hole deepened as well as lengthened and widened, while the sediment ridge flattened, widened and elongated in the downstream direction. Irrespective of time, the scaled scour depth (d_s/L_o) was larger for shallow flow depth (i.e. d_w/L_o = 0.76 to 1) and maximized at d_w/L_o = 1 (U_m/U_c = 0.75, run A6) (Figure 5 and Supporting Information S1). Compared to fully submerged flow (i.e. d_w/L_o = 4 and U_m/U_c = 0.71, run A10), d_s was on average 30% larger irrespective of experimental duration. For runs with a spherical obstacle (A11–A22), the typical obstacle mark morphology emerged only for run A16. Compared to run A6, d_s/L_o was on average 20% smaller, irrespective of experimental duration. For runs A11–A14, a wake-scour morphology composed of two lateral scour holes downstream of the obstacle emerged, while a frontal scour hole was absent. For runs A15, A17–A20 the same wake-scour morphology emerged at the beginning of experimental runs. However, with ongoing duration the morphology changed

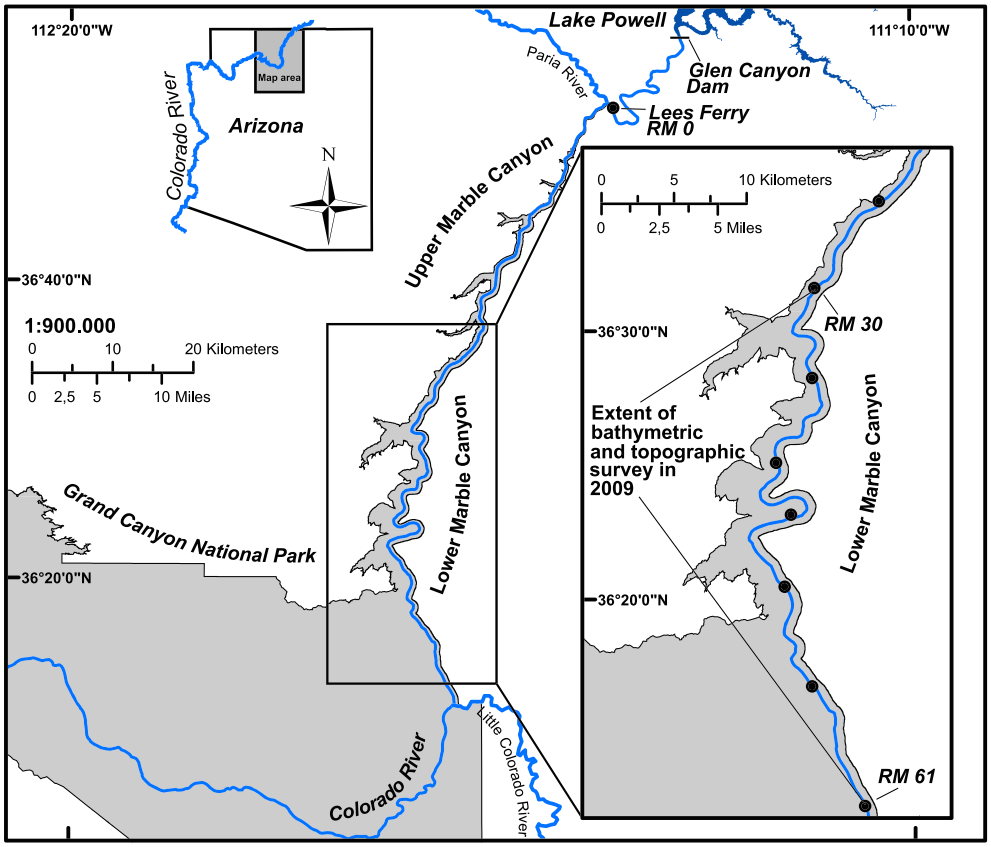

FIGURE 4 Map of Colorado River in the upstream portion of Grand Canyon National Park (shaded in grey) highlighting extent of bathymetric and topographic survey in lower marble canyon in 2009 (Kaplinski et al., 2017a). Distance between black dots in the study segment is 5 river miles. GIS data are provided by the U.S. Geological Survey and the Grand Canyon Monitoring and Research Center (GCMRC), while the illustration is inspired by 1Figure of Grams et al. (2019) [Colour figure can be viewed at wileyonlinelibrary.com]

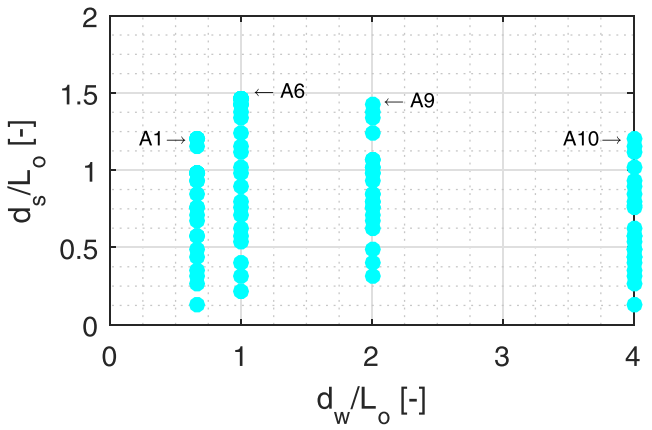

FIGURE 5 Scaled scour depth (d_s/L_o) against submergence ratio (d_w/L_o) irrespective of time exemplified for runs A1, A6, A9 and A10 [Colour figure can be viewed at wileyonlinelibrary.com]

slightly as a minor frontal scour hole emerged (approx. $t/t_e \sim$ 0.25–0.5), after exceeding a critical threshold of d_s/L_o (~0.2).

For runs A1–A10, A16, q^* showed an asymptotic (limiting) behaviour in time (Figure 6). Rapid incision and simultaneous enlargement of l_s and w_s occurred at the beginning (i.e. $t/t_e \leq 0.04$), which caused a high q^*. However, q^* decreased significantly for later stages of the experiments and could be approximated by power-law relationships for (i) longitudinal profiles and (ii) horizontal profiles of the frontal scour hole:

$$\text{(i)}\ q*(l_{sP}) = 6.0*10^{-6} * t/t_e{}^{-4.4} \left(\text{coefficient of determination}, R^2 = 0.60\right) \quad (8)$$

$$\text{(ii)}\ q*(w_{sP}) = 8.2*10^{-7} * t/t_e{}^{-5.7} \left(\text{coefficient of determination}, R^2 = 0.72\right) \quad (9)$$

It should be noted that $q^*(w_{sP})$ did not decrease to zero, because a slight enlargement in width was detected even for late stages of the experiments (i.e. $t/t_e \geq 0.7$).

3.2 | Influence of depth-limited alluvial layer

For series B, a typical obstacle mark pattern evolved for runs B1–B3 and B6, while a wake-scour morphology emerged for run B4. Due to the depth-limited alluvial layer, d_s/L_o, l_s/L_o and w_s/L were smaller compared to similar runs of series A (Figure 7a). Equilibrium conditions of d_s were attained earlier in time (for $U_m/U_c \geq 0.75$ at $t/t_e \sim$ 0.0005–0.0008, Figure 7c) as d_s reached the channel bottom. However, the enlargement of l_s and w_s continued (Figures 6 and 7d). An ANCOVA test (F-value = 0.67–0.69, p-value = 0.50–0.52) revealed that q^* over t/t_e for runs B1–B3 and B6 were not significantly different from those predicted by Equations (8) and (9). The dimensions of l_s/L_o and w_s/L_o were on average 30–40% larger for the angular obstacle ($Sh \geq 0.8$) compared to the spherical obstacle ($Sh \geq 0.6$).

3.3 | Impact of obstacle mobility

For series C, the typical obstacle mark pattern emerged for runs C1, C2 (Figure 7b) and C4 (Figure 7e), while the wake-scour morphology

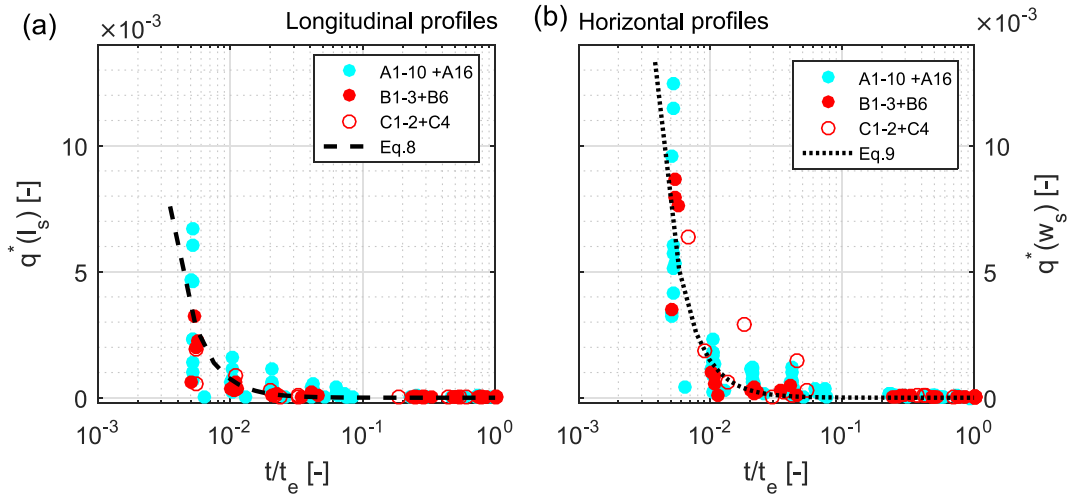

FIGURE 6 Scaled sediment transport rate over scaled time scale of all experimental series estimated from (a) upstream longitudinal profiles of the frontal scour hole and (b) upstream horizontal profiles of the frontal scour hole [Colour figure can be viewed at wileyonlinelibrary.com]

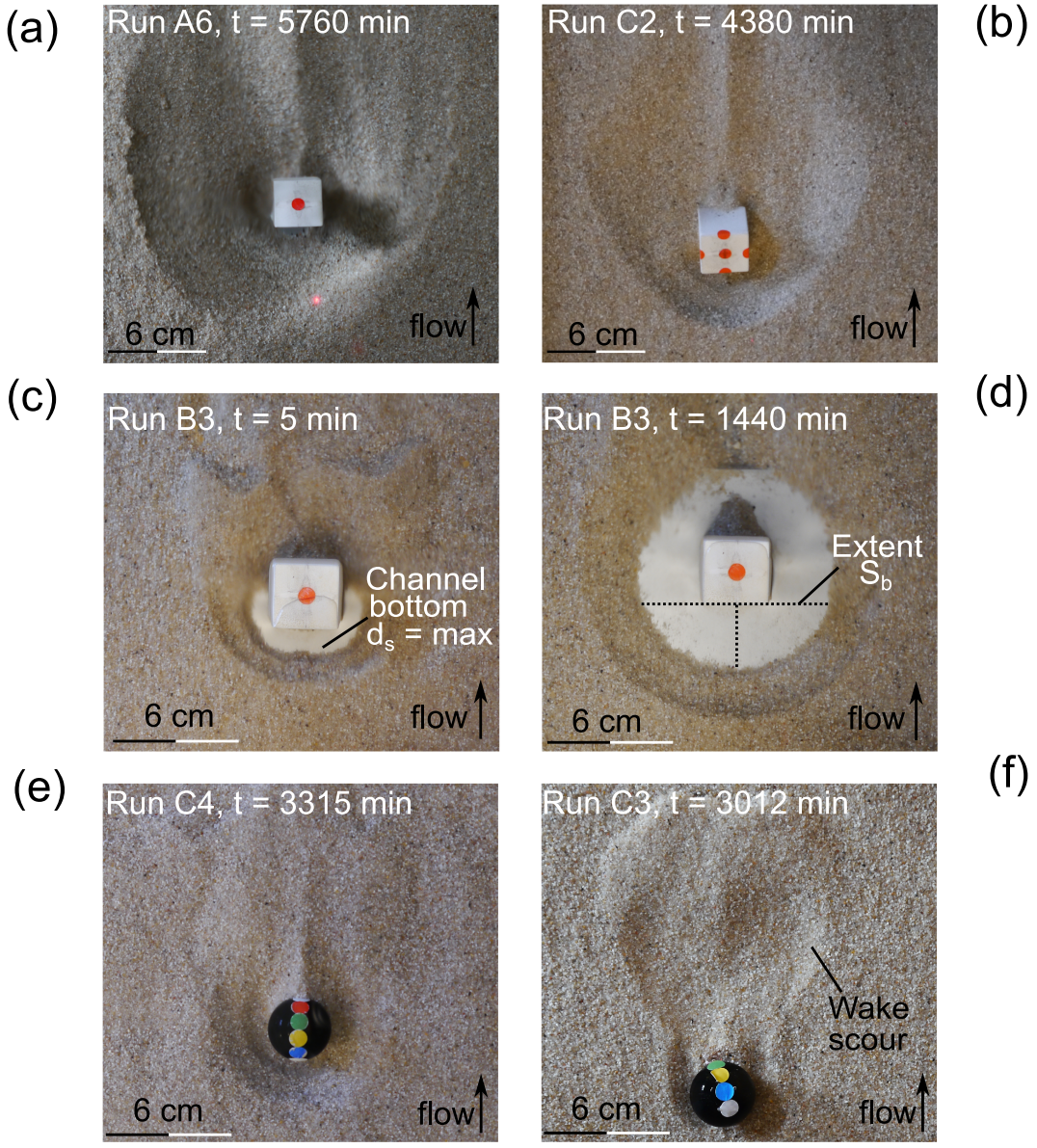

FIGURE 7 Plan view of frontal scour holes modelled at different stages of evolution and different experimental setups: (a) frontal scour hole at a mounted cube; (b) frontal scour hole at a moveable cube partially buried in the frontal scour hole and tilted into upstream direction; (c) frontal scour hole at an alluvial layer of reduced thickness after 5 min runtime indicating that scour incision reached flume bottom; (d) after 1440 min indicating ongoing enlargement of frontal scour hole in length, width as well as in the extent of scour hole bottom; (e) frontal scour hole at a moveable sphere partially buried in the frontal scour hole and tilted into upstream direction; (f) wake scour at a moveable sphere [Colour figure can be viewed at wileyonlinelibrary.com]

evolved for run C3 (Figure 7f). For runs C1 and C2, the scour incision undermined the obstacle and induced movement of the obstacle at $d_s/L_o \sim 0.2$ with respect to the regularly shaped obstacles used within this study. The movement was characterized by (i) upstream tilting of the obstacle relative to its origin position (i.e. x_0) against the direction of flow and (ii) self-burial of the obstacle (i.e. reduction of h_o relative to h_o at $t/t_e = 0$) (Figures 8a and b). Both processes show stepwise and asymptotic behaviour in time with rapid activity for $t/t_e < \sim 0.2$ irrespective of *Sh* (Figure 8c). Processes (i) and (ii) altered the obstacle's exposure to flow due to inclination of the obstacle's frontal face into the upstream direction (~20°), and by reducing the height of the obstacle protruding into the flow. Both processes significantly decelerated frontal scour hole incision in time, and reduced d_s/L_o by 15–20% on average compared to series A runs. q^* over t/t_e was not significantly different from Equations (8) and (9) (Figure 6) as l_s/L_o and w_s/L_o enlarged further in time.

3.4 | Obstacle marks at field scale

In total, 90 obstacle marks were identified along the study at boulders embedded in sand. A total of 83% of the boulders were located close to the channel banks and varied considerably in size relative to the ambient bed elevation (median h_o = 1 m, range h_o = 7 m; median w_o = 5 m, range w_o = 13 m). The boulder shapes ranged from quasi-rectangular to round. It should be noted that no significant inclination of the obstacle's frontal face against upstream direction could be detected, while the comparably low height of the obstacles in relation to the ambient streambed elevation suggests that obstacles were on the point of self-burial. Of the 90 obstacles, 89 obstacle marks were characterized by a clear definable frontal scour hole (i.e. typical obstacle mark pattern). However, it was challenging to determine the extent of the sediment ridge, mainly due to the presence of dunes in some segments of the study reach. For 92% of the identified frontal scour holes, an armour layer consisting of coarser sediment (i.e. gravel) in relation to the surrounding bed was present in S_b. The frontal scour holes were shallow compared to their l_s and w_s (Figures 9a–c, statistical properties provided in Table 2 and Supporting Information S2). Compared to absolute values of d_s, l_s and w_s for runs A1–A10 and A16, frontal scour hole dimensions are 50 to 100 times larger.

Although frontal scour holes at field scale were not as evenly developed as in the laboratory, shape similitude across spatial scales is obvious (Figures 7 and 10). Remarkably, one wake-scour pattern with only a minor frontal scour hole could be detected, similar to laboratory observations at a spherical obstacle (Figures 7f and 10b). Besides these two morphologies, no different spatial patterns of obstacle marks could be detected in the study section.

3.5 | Frontal scour hole geometry

Series A showed that the actual size of d_s/L_o in t/t_e depends on d_w/L_o and U_m/U_c (Figure 5). However, neglecting U_m/U_c, d_w/L_o and t/t_e, a monotonic increase and co-variation of l_s/L_o and w_s/L_o with increasing d_s/L_o is obvious (Figures 11a and b, Table 3). A co-variation of l_s/L_o and w_s/L_o with increasing d_s/L_o is also evident for the field data, although there is a larger range of boulder sizes (L_o) compared to the experimental series. L_o particularly controls the size of the frontal scour hole, which is also present for the field data (Figures 11g and h).

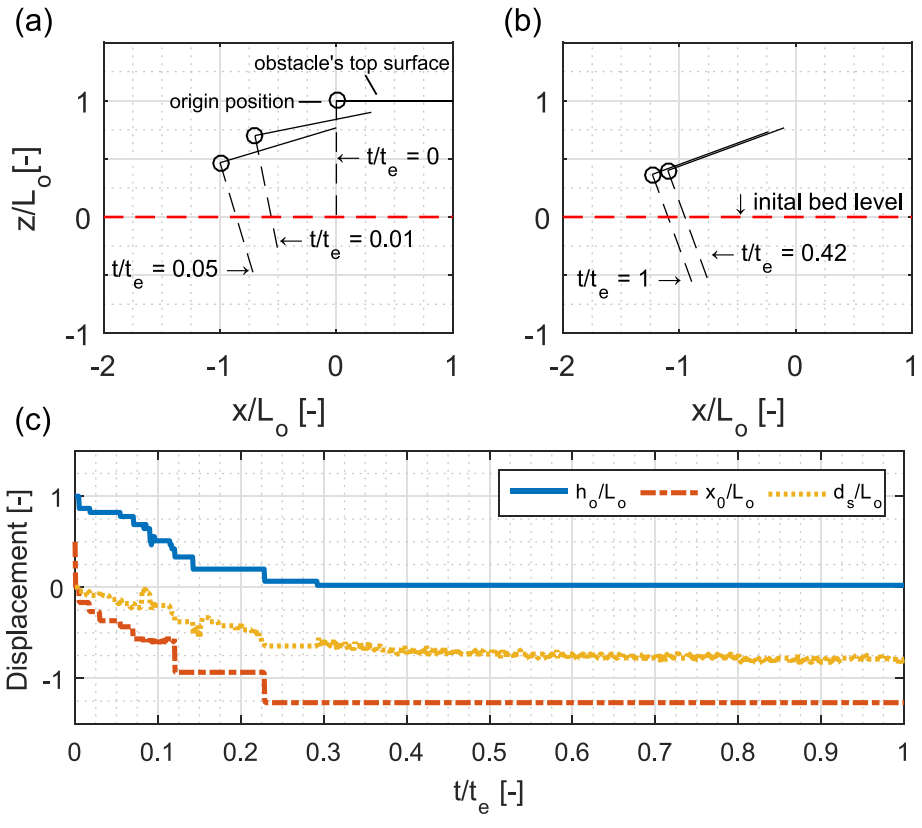

FIGURE 8 Movement (self-burial and upstream tilting) at a cuboid obstacle (run C1) for (a) initial phase of experiments ($t/t_e \leq 0.05$) and (b) for final phase of experiments ($t/t_e \geq 0.42$). (c) Trajectory of non-dimensional obstacle movement and scour depth evolution over non-dimensional time observed at run C4 (spherical obstacle) [Colour figure can be viewed at wileyonlinelibrary.com]

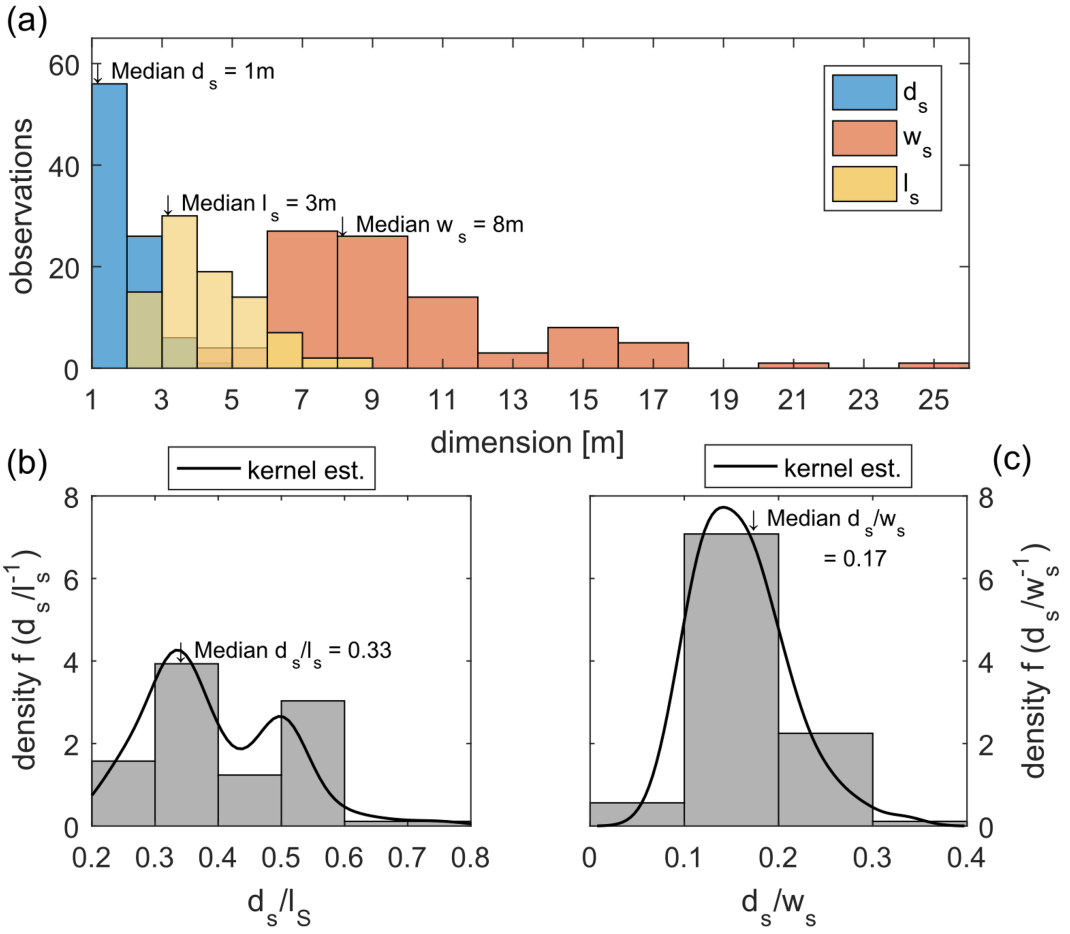

FIGURE 9 (a) Histogram of absolute scour hole dimensions (d_s, l_s, w_s) at field evidence. (b) Histogram of morphometric relation (d_s/l_s) including kernel density estimation. (c) Histogram of morphometric relation (d_s/w_s) including kernel density estimation [Colour figure can be viewed at wileyonlinelibrary.com]

TABLE 2 Statistical properties of absolute values of morphometric variables at field evidence (n = 89)

Parameter	Median	Mean	IQR	MAD
d_s [m]	1	1.47	1	0.59
l_s [m]	3	3.80	2	1.16
w_s [m]	8	9.35	4	2.73

IQR = interquartile range, MAD = median absolute deviation.

However, the estimated $ß_1$ of the relationships l_s/L_o and w_s/L_o on d_s/L_o (Table 3) indicate long and wide frontal scour holes that are relatively shallow.

The same applies to series B and C. For series B, d_s/L_o depended solely on d_{sed}/L_o, while frontal scour holes were wider and longer in relation to their shallow depth and a considerable deviation of l_s/L_o and w_s/L_o on d_s/L_o for t/t_e = 1 existed (Figures 11c and d). For series C, obstacle tilting and self-burial caused smaller values of d_s, l_s and w_s compared to series A (Figures 11e and f).

3.6 | Similitude of frontal scour hole geometry

For series A, the scaled profiles of the frontal scour collapsed into a narrow band, irrespective of hydraulic conditions and time (Figures 12a and b).

Superimposed profiles were also present for series B and C experiments, irrespective of hydraulic conditions and time (Figures 12c–f). However, for series B experiments the scour bottom (S_b) was significantly wider compared to series A results (Figures 7c and d), while for series C experiments S_b could not be detected due to the tilting of the obstacles.

For the field evidence, scaled profiles of the frontal scour holes do not properly collapse in a common form (Figures 12g and h), as considerable differences in slope inclination were present. However, for the 89 frontal scour holes, the median inclination of the longitudinal scour slope was 23°, and 75% of the slopes were less than 28°. The median inclination of the horizontal scour slope was 18°, and 75% of the slopes were less than 24° (Figure 12i). Unfortunately, no differentiation between upper and lower slope could be made based on the derived profiles.

3.7 | Geometric relations in time at laboratory scale

Geometric relations (i.e. d_s/l_s and d_s/w_s) were not constant over time, and show a piecewise linear pattern that is composed of a systematic increase in d_s/l_s and d_s/w_s for t/t_e < 0.04, followed by a decreasing tendency for $t/t_e \geq 0.04$ (Figure 13).

For series B experiments, d_s/l_s and d_s/w_s were on average 19–23% smaller compared to runs A1–A10 and A16, but showed the

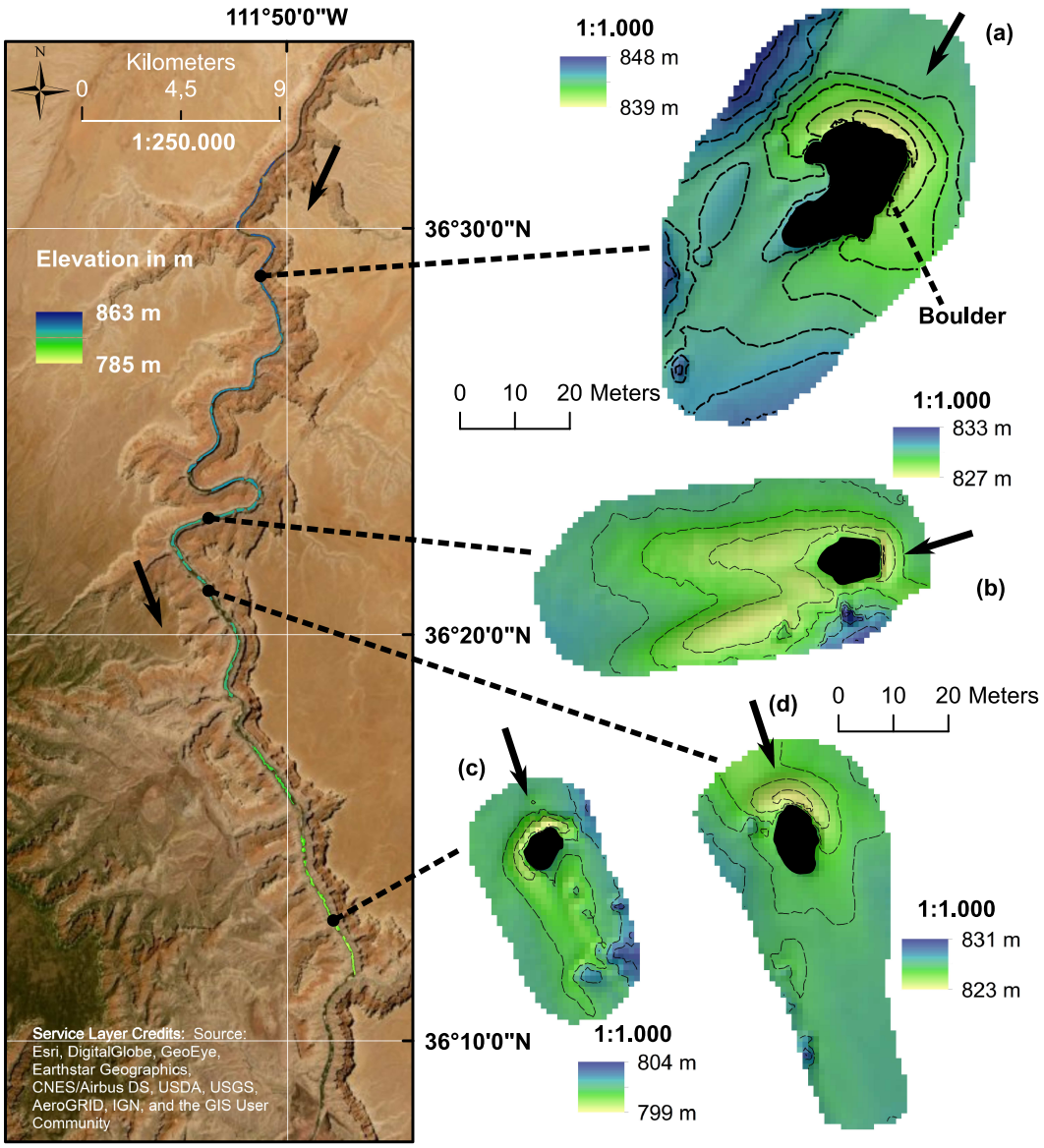

FIGURE 10 Examples of obstacle mark morphologies at boulders of different size identified within the study area. (a, c, d) Typical obstacle mark morphologies; (b) wake scour pattern. Isoline interval is 1 m and arrows indicate direction of flow. Boulders are highlighted in black. Complete overview field evidence including coordinates is provided as supporting information [Colour figure can be viewed at wileyonlinelibrary.com]

same piecewise linear pattern plotted against $\log_{10}(t/t_e)$, while for series C obstacle tilting in the upstream direction caused a relocation of the frontal scour hole, producing relatively high values of d_s/l_s for $t/t_e < 0.04$ as the size of l_s was then comparable to d_s.

To account for the time-series character of the dataset and in order to achieve stationarity as a requirement for statistical modelling, d_s/l_s and d_s/w_s of series A, B and C were detrended by subtracting the mean. Upon application of bootstrapped regression (Davison & Hinkley, 2009) to the detrended data, three different slope coefficients β_1 on d_s/l_s and d_s/w_s over $\log(t/t_e)$ were estimated (solid lines in Figure 13):

i. $t/t_e \leq 0.002$–0.003 rapid incision (β_1 for $d_s/l_s = 0.17$; β_1 for $d_s/w_s = 0.09$).
ii. $0.003 < t/t_e < 0.04$ decreasing rate of incision (β_1 for $d_s/l_s = 0.01$; β_1 for $d_s/w_s = 0.05$).
iii. $t/t_e \geq 0.04$ a significant break-point is present, for which the frontal scour hole deepening ceases, while slight widening occurs (β_1 for $d_s/l_s = -0.01$; β_1 for $d_s/w_s = -0.03$).

4 | INTERPRETATION OF LABORATORY RESULTS AND FIELD EVIDENCE

4.1 | Process dynamics of scour hole enlargement

The deepening and sediment mobilization within the inner frontal scour hole caused an expansion of S_b/L_o with t/t_e and d_s/L_o (Figures 14a and b). The sediment loss in the inner scour hole destabilized the upper longitudinal frontal scour hole slope and caused intermittent gravitational movements in time. Considering all experimental series, the inclination (Φ) of the upper longitudinal frontal

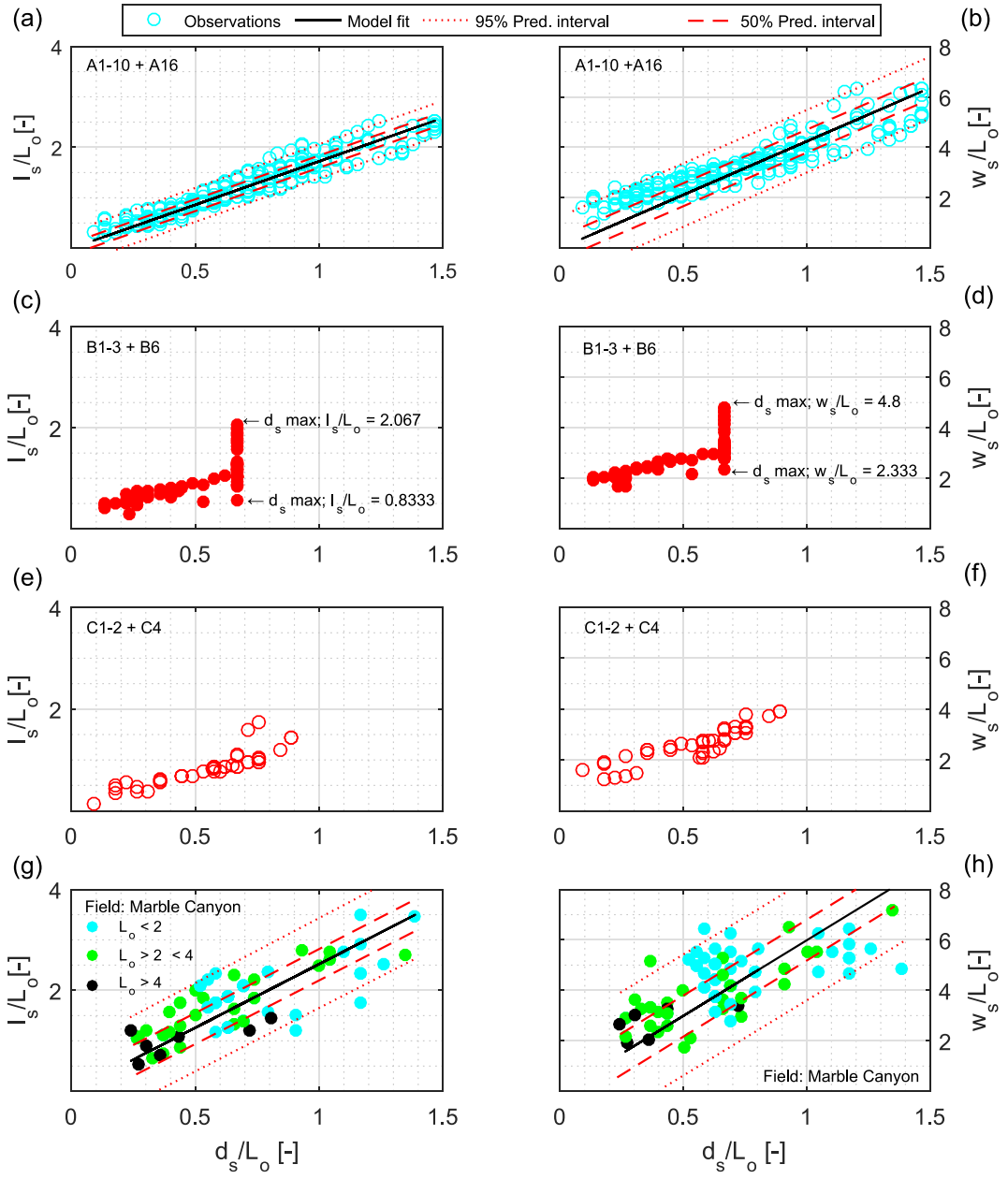

FIGURE 11 Linear relationships of non-dimensional morphometric variables of the frontal scour hole. (a) l_s/L_o against d_s/L_o for series A, slope $ß_1$ of the relationship is depicted in Table 3. (b) w_s/L_o against d_s/L_o for series A, slope $ß_1$ of the relationship is depicted in Table 3. (c) l_s/L_o against d_s/L_o for series B. (d) w_s/L_o against d_s/L_o for series B. (e) l_s/L_o against d_s/L_o for series C. (f) w_s/L_o against d_s/L_o for series C. (g) l_s/L_o against d_s/L_o for field evidence, slope $ß_1$ of the relationship is depicted in Table 3. (h) w_s/L_o against d_s/L_o for field evidence, slope $ß_1$ of the relationship is depicted in Table 3 [Colour figure can be viewed at wileyonlinelibrary.com]

TABLE 3 Statistical properties of linear regression ($y = ß_1x$) for laboratory (n = 231) and field results (n = 89) on non-dimensional morphometric variables

Model fit	R^2	$ß_1$	95% confidence interval for $ß_1$	RMSE of model fit
$l_s/L_o = ß_1 d_s/L_o$ (series A)	0.93	1.72‡	1.70, 1.75	0.17
$l_s/L_o = ß_1 d_s/L_o$ (field evidence)	0.69	2.52‡	2.39, 2.65	0.44
$w_s/L_o = ß_1 d_s/L_o$ (series A)	0.85	4.24‡	4.14, 4.34	0.63
$w_s/L_o = ß_1 d_s/L_o$ (field evidence)	0.63	5.99‡	5.63, 6.35	1.22

‡Bootstrapped estimates.

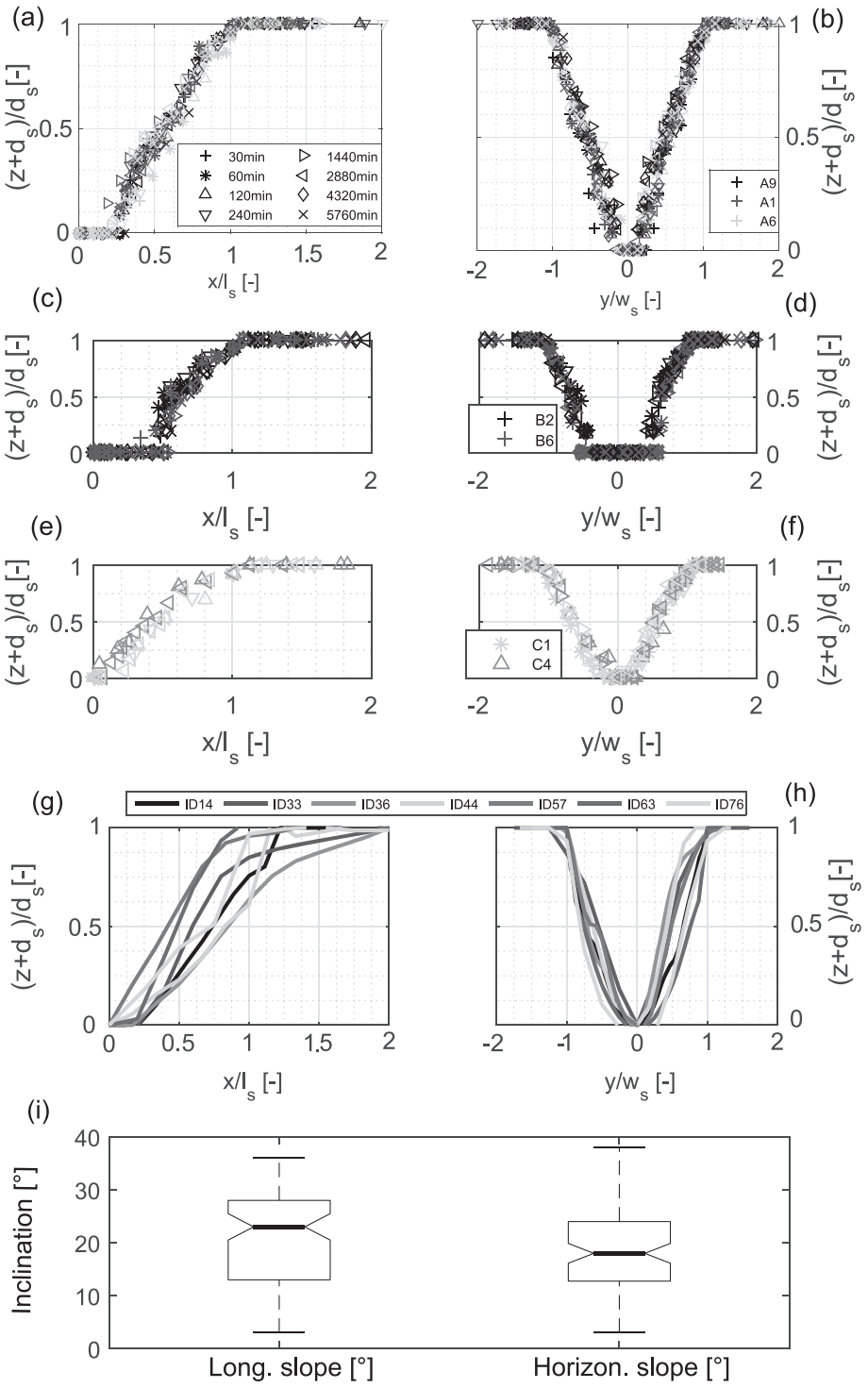

FIGURE 12 (a) Scaled longitudinal frontal scour hole profiles exemplified for runs A1, A6 and A9 at indicated times (a), runs B2 and B6 (c), and runs C1 and C4 (e). Scaled horizontal frontal scour hole profiles of runs A1, A6 and A9 (b), runs B2 and B6 (d), and runs C1 and C4 (f). (g) Scaled longitudinal frontal scour hole profiles at boulders of different size. (h) Scaled horizontal frontal scour hole profiles at boulders of different size. (i) Inclination of longitudinal and horizontal scour hole slopes for all field evidence (n = 89)

scour hole slope showed a decreasing tendency with $\Phi > \Phi_{crit}$ for $t/t_e < 0.04$ and $\Phi \leq \Phi_{crit}$ for $t/t_e \geq 0.04$ (Figure 14c), while Φ of the lower slope was by tendency $>\Phi_{crit}$ irrespective of time and experimental series (Figure 14e). Although a decreasing tendency of Φ with time is also present for the upper horizontal frontal scour hole slope (Figure 14d), Φ of the lower slope remained considerably steep over the experimental duration (Figure 14f).

4.2 | Quantitative models of enlargement

Two mechanistic models are proposed to assess the enlargement of l_s and w_s based on (i) d_s, (ii) co-tangent of upper slope inclination ($\tan^{-1}(\Phi)$), and (iii) span of the scour hole bottom (S_b). The models were constructed upon the log-transformed data of all experimental series and the field evidence using bootstrapped regression for insensitivity to outliers (Figure 15a for l_s; Figure 16c for w_s; Table 4 for statistical properties). Accordingly, l_s can be estimated by

$$\log_{10}(l_s) = 0.88 * \log_{10}(d_s * \cot\Phi + S_b) \quad (10)$$

The analysis of w_s with regard to (i), (ii) and (iii) is complemented by a constant, resulting from the relationship of l_s to w_s, indicating that w_s is approximately 2.4 times l_s (Figures 16a and b). However, for a conservative approximation of w_s, the constant 2 is used:

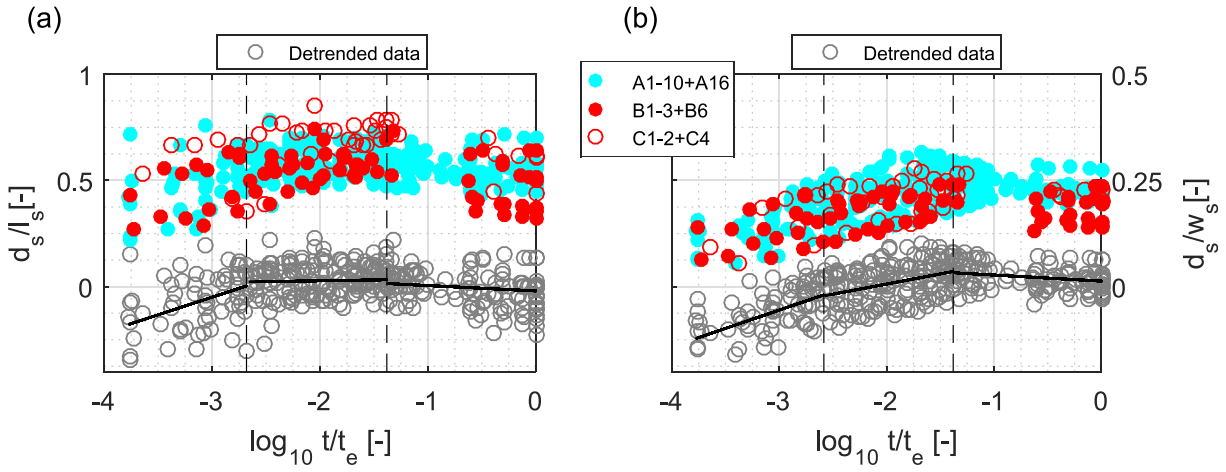

FIGURE 13 Geometric relations of the frontal scour hole over non-dimensional time in $\log_{10}$ scale for all experimental series (a) d_s/l_s and (b) d_s/w_s [Colour figure can be viewed at wileyonlinelibrary.com]

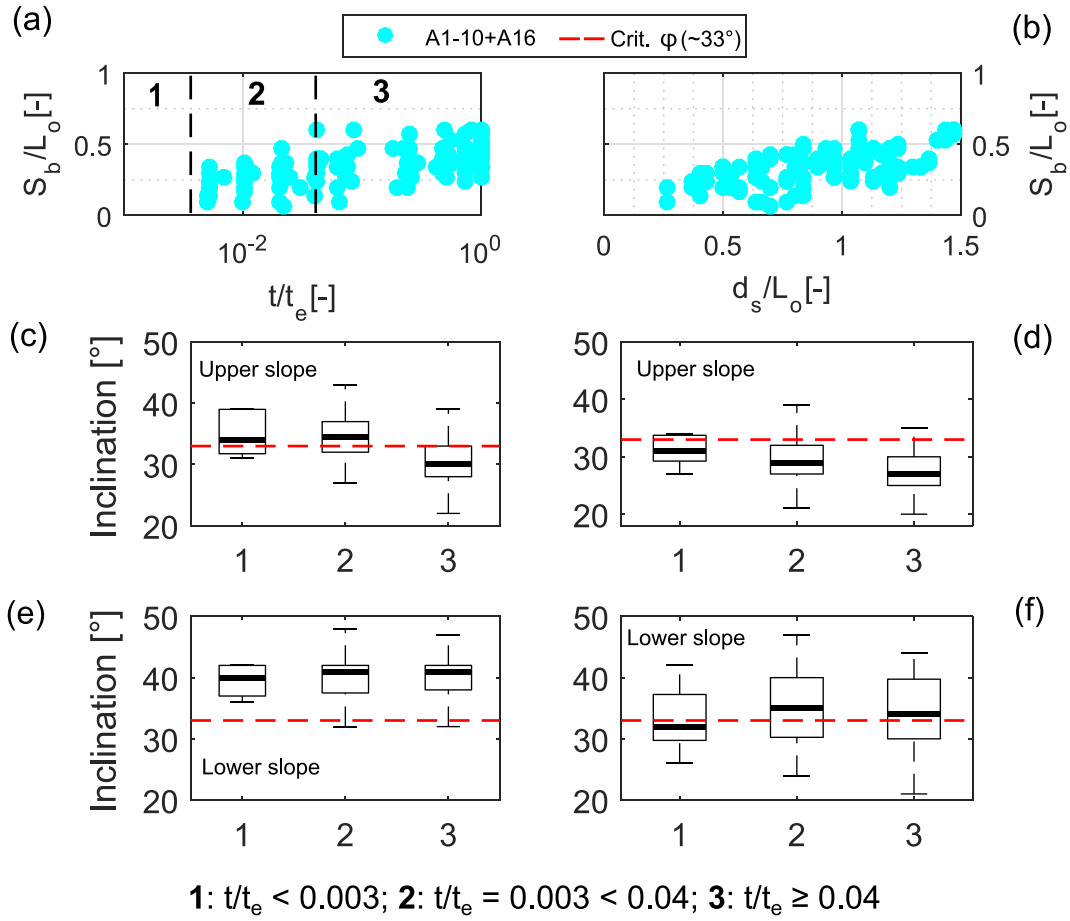

FIGURE 14 (a) Scaled scour bottom against non-dimensional time (**1**: $T/t_e < 0.003$; **2**: = 0.003 < 0.04; **3**: ≥ 0.04. (b) Scaled scour bottom against scaled scour depth. (c) Inclination of upper slope segment (n = 174) of the frontal scour hole estimated from longitudinal profiles grouped by non-dimensional time (**1**: $T/t_e < 0.003$; **2**: = 0.003 < 0.04; **3**: ≥ 0.04). (d) from horizontal scour hole profiles (n = 176). (e) Inclination of lower slope segment (n = 157) of the frontal scour hole estimated from longitudinal profiles grouped by non-dimensional time. (f) From horizontal profiles (n = 109) [Colour figure can be viewed at wileyonlinelibrary.com]

$$\log_{10}(w_s) = 1.32 * \log_{10}(2 * d_s * \cot\Phi + S_b) \quad (11)$$

Equations (10) and (11) show reasonable agreement in comparison to observations on l_s and w_s for experimental data and field evidence (Figures 15b and 16d).

5 | DISCUSSION OF LABORATORY RESULTS AND FIELD EVIDENCE

Our findings can be interpreted in light of the experimental hydraulic data presented by Schlömer et al. (2020), who have attributed the

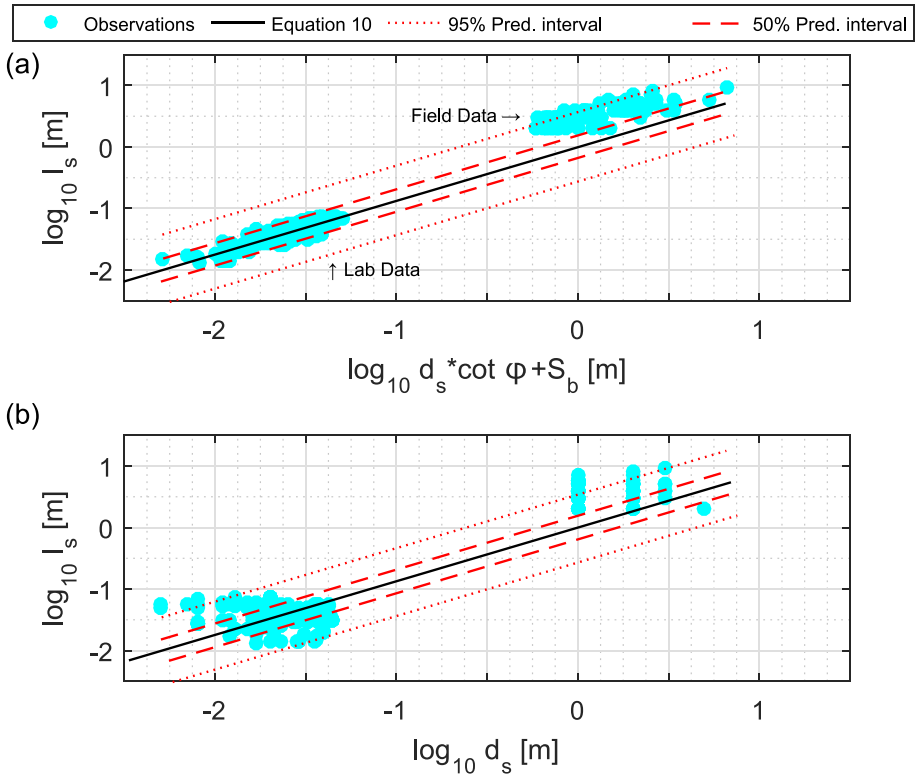

FIGURE 15 (a) Log-transformed l_s of laboratory data and field evidence against log-transformed model values. (b) Log-transformed l_s against log-transformed d_s for laboratory data and field evidence [Colour figure can be viewed at wileyonlinelibrary.com]

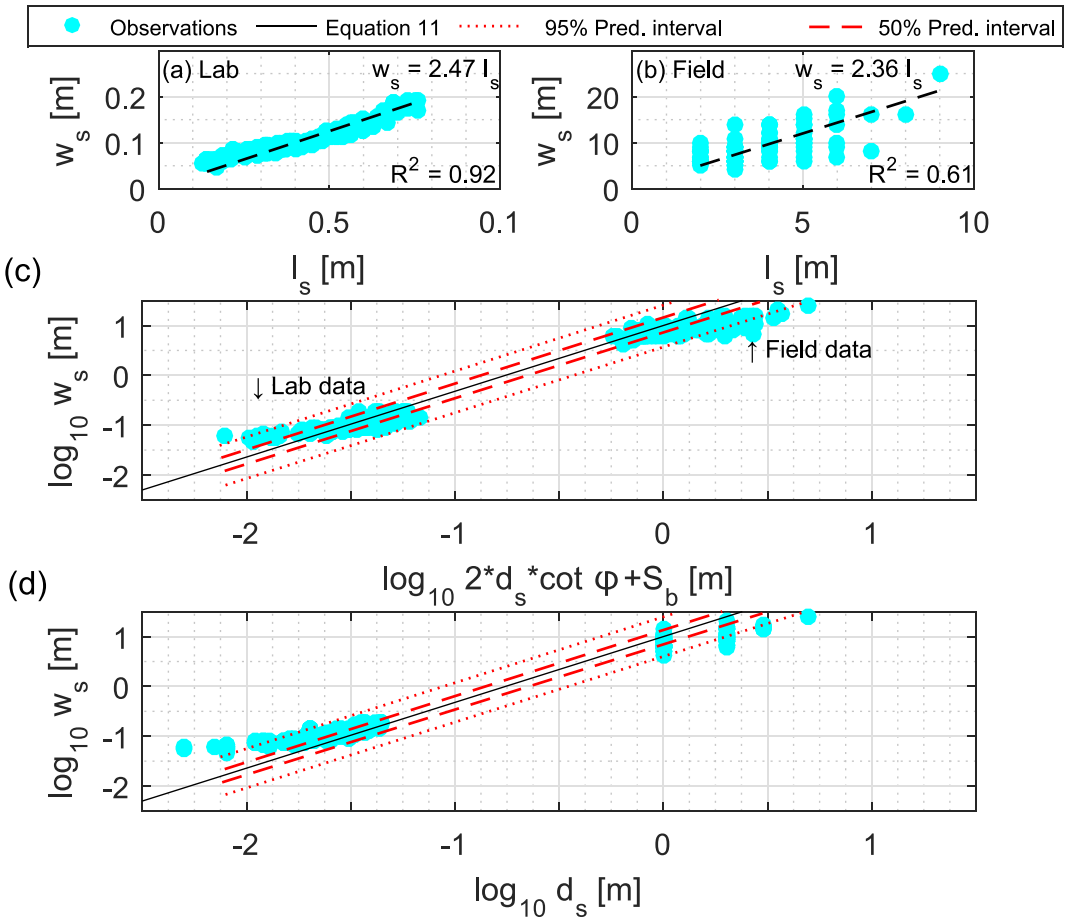

FIGURE 16 Linear relationships of l_s against w_s for (a) laboratory data and (b) field evidence. (c) Log-transformed w_s of laboratory data and field evidence against log-transformed model values. (d) Log-transformed w_s against log-transformed d_s for laboratory data and field evidence [Colour figure can be viewed at wileyonlinelibrary.com]

TABLE 4 Statistical properties of model fits (linear regressions (y = ß$_1$x)) on non-dimensional morphometric variables (n = 320)

Model fit	R^2	ß$_1$	95% confidence interval for ß$_1$	RMSE of model fit
$\log_{10}(l_s)$	0.88	0.88	(0.85, 0.90)	0.284
$\log_{10}(w_s)$	0.95	1.32	(1.30, 1.34)	0.2042

maximization of d_s/L_o at d_w/L_o to a high vertical pressure gradient at the obstacle front that creates an intense downflow and efficient HV system. During scour incision, HV1 and HV2 subside into the frontal scour hole where HV1 expands in diameter, indicated by an expansion of S_b/L_o with t/t_e and d_s/L_o. Due to the expansion in diameter, the shear stress beneath the vortex decreases and equilibrium of incision is approached (cf. Kothyari et al., 1992). Thus, hydraulic processes and morphology are connected in time and characterized by feedback loops that indicate a self-organizing behaviour (Coco & Murray, 2007), while S_b/L_o can be interpreted as a proxy for the size of HV1.

The enlargement of l_s/L_o and w_s/L_o is directly coupled to d_s/L_o as the scour incision undermines the scour hole slopes and induces gravitational movements. The lower slope is governed by the rotation of HV1 and by tendency stabilized at $\Phi > \Phi_{crit}$, while the upper slope adjusts to the angle of repose by gravitational movements, indicating a positive feedback loop between scour incision and enlargement in l_s/L_o. Furthermore, the enlargement of w_s can be attributed to the convection of detached shear layers from the legs of HV1 at the lateral sides of the obstacle, resulting in strong amplification of shear stress at the bed as shown by Kirkil and Constantinescu (2010) and Kirkil et al. (2008).

Thus, experimental results support working hypothesis (A), while similar observations are reported by Bateman et al. (2006) and Chreties et al. (2008, 2013) for the geometry of frontal scour holes at emergent bridge piers.

The observed wake scouring has to be attributed to recirculation of approaching flow and turbulence-induced high shear stress in the near-wake, while the rounded shape of the obstacle inhibits significant downflow at the obstacle frontal face and causes a small HSV. As described by Schlömer et al. (2020), the wake scouring occurs at round-shaped obstacles only at high submergence (i.e. $d_w/L_o > 1.6$). Remarkably, the wake-scouring pattern was also observed for the field evidence and it is supposed that the same hydraulic processes were responsible.

For the field evidence, the wider scatter of l_s/L_o and w_s/L_o for a given d_s indicates long and wide frontal scour holes that are relatively shallow, in agreement with Butch (1991, 1999), who reported w_s to be 4.7 times d_s based on measurements of frontal scour holes at bridge piers.

The sensitivity of d_s was confirmed by series B and C, indicating that scour depth incision (i) depended on the thickness of the alluvial layer, supporting working hypothesis (B), and (ii) was damped by obstacle tilting and self-burial, supporting working hypothesis (C).

The assumption of a depth-limited alluvial layer ($d_{sed}/L_o \leq 1$) for the field data is reasonable based on indications given by Hazel et al. (2006), who reported an average sediment thickness in the main channel of ~1 m (supported by unpublished 2016 measurements of sand thicknesses using sub-bottom profiling sonar). Hence, the mean value of d_s (i.e. 1 m) can be interpreted as a conservative estimate for the thickness of the alluvial layer in Marble Canyon at the time of the survey, while $d_{sed}/L_o \leq 1$ suggests a plausible explanation for the comparable shallow frontal scour holes. However, fluctuations of the sediment thickness are known, primarily induced by sediment input from tributaries that is subsequently redistributed during controlled floods (Grams et al., 2019). Thus, general bedload sediment mobilization ($U_m/U_c > 1$) occurs at least intermittently if not under most flows, indicated by the presence of near-ubiquitous dunes and the low-stage bedform migration measurements reported by Leary and Buscombe (2020) in a similar downstream reach. Consequently, regular sediment transport into the frontal scour hole results in partial filling and reduction in d_s (Hong et al., 2017). Moreover, the armour layer that was detected in 92% of the frontal scour holes prevents further scour incision, similar to the physical effects of $d_{sed}/L_o < 1$.

5.1 | Shortcomings in comparing field evidence and laboratory results

The frontal scour holes observed in the field must be treated as 'snapshots' in time that emerged during unsteady hydraulics, while information on these hydraulic boundary conditions and the time scale of the scouring is unknown.

However, even though laboratory studies were conducted at reduced complexity, the scale-invariance of frontal scour hole geometry documented here, in which morphological details (i.e. S_b) are persistent, lends credence to laboratory–field comparisons. Unfortunately, not every small morphological detail could be identified (i.e. knickpoint in scour slopes) in the field data, due to the 1 m resolution of the DEM. However, the comparison of field evidence and laboratory results revealed similitude of equifinal form. However, the equilibrium time scale of frontal scouring is reported to be similar in sub-prototype-scale laboratory studies and prototype field conditions (e.g. Sutherland & Soulsby, 2011), which does not imply equifinality of the process. Despite the scatter, likely due to the migration of bedforms as discussed above, the co-variation of l_s/L_o and w_s/L_o with increasing d_s/L_o revealed in both laboratory and field results is reasonably strong evidence that the specific scouring processes identifiable from the laboratory results also occur at prototype scale, resulting in similitude of form. The determination of a near-equilibrium condition is therefore attributed to the sediment transport rate out of the frontal scour hole, which should average approximately zero over time. The laboratory results have shown that the sediment transport rate approaches near equilibrium conditions, while the relation of d_s/l_s and d_s/w_s enabled the determination of temporal evolution phases.

Although the field evidence implies scour-hole persistence for the given boundary conditions, statements on the temporal evolution stage of field evidence are not possible.

6 | CONCLUSION AND OUTLOOK

Recalling the aims formulated in the Introduction, the following conclusions can be drawn:

i. The enlargement of the frontal scour hole in time is triggered by depth incision, steepening of slopes and gravitational movements at the scour slopes, irrespective of hydraulic boundary conditions. Three temporal evolution phases could be determined based on the relations d_s/l_s and d_s/w_s that are supported by the asymptotic sediment transport rate out of the frontal scour hole in time. A quantitative model is formulated that assesses enlargement in local scour length and width based on scour depth, the inclination of frontal scour slopes and the span of the scour hole bottom irrespective of scale, which can be applied to estimate the spatial extent of countermeasures for local scour protection.
ii. The depth of the frontal scour at boulder-like obstructions is impacted by limiting boundary conditions that are supposed to be plausible at field conditions (i.e. boulder tilting and burial, limitations due to the thickness of the alluvial layer, armouring effects as well as infilling of incoming sediments), making d_s a sensitive morphometric parameter.
iii. Integration of laboratory results and field evidence on obstacle marks demonstrates a scale invariance that implies similitude of processes and form.

However, more complex scenarios have to be addressed in upcoming laboratory research to bridge the gap between simulated obstacle marks and their real-world counterparts. In particular, the impact of unsteady discharge, unsteady upstream sediment supply, and the effects of discharge chronologies and exceedances, to test the consistency of observations on the temporal evolution of geometric relations (d_s/l_s, d_s/w_s) under these conditions, and the quantitative model presented here for frontal scour hole enlargement.

Field evidence revealed that frontal scour holes at large boulders are distinguishable from other sedimentary structures and have preservation potential under complex boundary conditions. However, obstacle marks are ephemeral in the sense that they persist only as long as the obstacle that creates them. Thus, they are a suitable indicator for the evaluation of sediment supply and net change in thickness of the alluvial layer (Δd_{sed}). An extremely large sediment supply (i.e. $\Delta d_{sed} >> \Delta d_s$) would result in a significant reduction of d_s, burial of the obstacle and complete disappearance of the obstacle mark.

ACKNOWLEDGEMENTS

The Marble Canyon field data are available in Kaplinski et al. (2017b) and were collected with support provided by the Glen Canyon Dam Adaptive Management Program administered by the U.S. Department of the Interior Bureau of Reclamation. Dr Taylor Rowley, Dr Rebecca Hodge and an anonymous reviewer provided thorough and constructive comments on previous drafts of this manuscript, which are gratefully acknowledged. Any use of trade, firm or product names is for descriptive purposes only and does not imply endorsement by the U.S. Government.

Open access funding enabled and organized by Projekt DEAL.

CONFLICT OF INTEREST STATEMENT

The authors declare that they have no conflict of interest.

DATA AVAILABILITY STATEMENT

The Marble Canyon field data are available in Kaplinski et al. (2017b).

Experimental and field results are available in the supporting information attached to this manuscript.

The full experimental dataset is available on request from the corresponding author.

REFERENCES

Allen, J.R.L. (1982) *Sedimentary Structures, their Character and Physical Basis*. Elsevier: Burlington, VA.

Baker, V.R. & Bunker, R.C. (1985) Cataclysmic Late Pleistocene flooding from glacial Lake Missoula: A review. *Quaternary Science Reviews*, 4 (1), 1–41. https://doi.org/10.1016/0277-3791(85)90027-7

Barenblatt, G.I. (2003) *Scaling*. Cambridge University Press: Cambridge.

Bateman, A., Fernández, M. & Parker, G. (2006) Morphodynamic model to predict temporal evolution of local scour in bridge piers. In: Parker, G. & García, M.H. (Eds.) *River, Coastal and Estuarine Morphodynamics: RCEM 2005. Proceedings of the 4th IAHR Symposium on River, Coastal and Estuarine Morphodynamics, 4–7 October 2005, Urbana, IL, USA*. London: Taylor & Francis, pp. 911–920.

Bauri, K.P. & Sarkar, A. (2016) Flow and scour around vertical submerged structures. *Sādhanā*, 41(9), 1039–1053. https://doi.org/10.1007/s12046-016-0539-y

Baynes, E.R.C., van de Lageweg, W.I., McLelland, S.J., Parsons, D.R., Aberle, J., Dijkstra, J. *et al*. (2018) Beyond equilibrium: Re-evaluating physical modelling of fluvial systems to represent climate change. *Earth-Science Reviews*, 181, 82–97. https://doi.org/10.1016/j.earscirev.2018.04.007

Bouratsis, P., Diplas, P., Dancey, C.L. & Apsilidis, N. (2017) Quantitative spatio-temporal characterization of scour at the base of a cylinder. *Water*, 9(3), 227. https://doi.org/10.3390/w9030227

Bouratsis, P., Diplas, P., Dancey, C.L. & Apsilidis, N. (2013) High-resolution 3-D monitoring of evolving sediment beds. *Water Resources Research*, 49(2), 977–992. https://doi.org/10.1002/wrcr.20110

Boyer, C. & Roy, A.G. (1991) Morphologie du lit autour d'un obstacle soumis à un écoulement en couche mince. *Géographie Physique et Quaternaire*, 45(1), 91–99.

Breusers, H.N.C. & Raudkivi, A.J. (1991) *Scouring*. Rotterdam: Balkema.

Buscombe, D., Grams, P.E. & Kaplinski, M.A. (2014a) Characterizing riverbed sediment using high-frequency acoustics: 1. Spectral properties of scattering. *Journal of Geophysical Research - Earth Surface*, 119(12), 2674–2691. https://doi.org/10.1002/2014JF003189

Buscombe, D., Grams, P.E. & Kaplinski, M.A. (2014b) Characterizing riverbed sediment using high-frequency acoustics: 2. Scattering signatures of Colorado River bed sediment in marble and grand canyons. *Journal of Geophysical Research - Earth Surface*, 119(12), 2692–2710. https://doi.org/10.1002/2014JF003191

Buscombe, D., Grams, P.E. & Kaplinski, M.A. (2017) Compositional signatures in acoustic backscatter over vegetated and unvegetated mixed sand–gravel riverbeds. *Journal of Geophysical Research - Earth Surface*, 122(10), 1771–1793. https://doi.org/10.1002/2017JF004302

Butch, G.K. (1991) *Measurement of Bridge Scour at Selected Sites In New York, Excluding Long Island: Water Resources Investigations Report 91-4083*. Albany, NY: USGS/New York State Department of Transportation.

Butch, G.K. (1999) Scour-hole dimensions at selected bridge piers in New York. In: Richardson, E.V. & Lagasse, P.F. (Eds.) *Stream Stability and Scour at Highway Bridges*. Reston, VA: ASCE, pp. 557–566.

Carling, P.A., Kirkbride, A.D., Parnachov, S., Borodavko, P.S. & Berger, G.W. (2002) Late Quaternary catastrophic flooding in the Altai mountains of south–central Siberia: A synoptic overview and an introduction to flood deposit sedimentology. In: Garzón, G., Martini, I.P. &

Baker, V.R. (Eds.) *Flood and Megaflood Processes and Deposits: Recent and Ancient Examples*. Malden, MA: Blackwell Science, pp. 17–35.

Carling, P.A. & Reader, N.A. (1982) Structure, composition and bulk properties of upland stream gravels. *Earth Surface Processes and Landforms*, 7(4), 349–365. https://doi.org/10.1002/esp.3290070407

Chen, Q., Qi, M., Zhong, Q. & Li, D. (2017) Experimental study on the multimodal dynamics of the turbulent horseshoe vortex system around a circular cylinder. *Physics of Fluids*, 29(1), 15106. https://doi.org/10.1063/1.4974523

Chen, Q., Yang, Z. & Wu, H. (2019) Evolution of turbulent horseshoe vortex system in front of a vertical circular cylinder in open channel. *Water*, 11(10), 2079.

Chou, J.H. & Chao, S.Y. (2000) Branching of a horseshoe vortex around surface-mounted rectangular cylinders. *Experiments in Fluids*, 28(5), 394–402. https://doi.org/10.1007/s003480050399

Chreties, C., Simarro, G. & Teixeira, L. (2008) New experimental method to find equilibrium scour at bridge piers. *Journal of Hydraulic Engineering*, 134(10), 1491–1495. https://doi.org/10.1061/(ASCE)0733-9429(2008)134:10(1491)

Chreties, C., Teixeira, L. & Simarro, G. (2013) Influence of flow conditions on scour hole shape for pier groups. *Proceedings of the Institution of Civil Engineers: Water Management*, 166(3), 111–119. https://doi.org/10.1680/wama.11.00054

Cin, R.D. (1968) "Pebble clusters": Their origin and utilization in the study of palaeocurrents. *Sedimentary Geology*, 2(4), 233–241. https://doi.org/10.1016/0037-0738(68)90001-8

Coco, G. & Murray, A.B. (2007) Patterns in the sand: From forcing templates to self-organization. *Geomorphology*, 91(3–4), 271–290. https://doi.org/10.1016/j.geomorph.2007.04.023

Comiti, F., Andreoli, A. & Lenzi, M.A. (2005) Morphological effects of local scouring in step–pool streams. *Earth Surface Processes and Landforms*, 30(12), 1567–1581. https://doi.org/10.1002/esp.1217

Dargahi, B. (1989) The turbulent flow field around a circular cylinder. *Experiments in Fluids*, 8(1–2), 1–12. https://doi.org/10.1007/BF00203058

Dargahi, B. (1990) Controlling mechanism of local scouring. *Journal of Hydraulic Engineering*, 116(10), 1197–1214. https://doi.org/10.1061/(ASCE)0733-9429(1990)116:10(1197)

Davison, A.C. & Hinkley, D.V. (2009) *Bootstrap Methods and their Application*. Cambridge: Cambridge University Press.

Dey, S. (2014) *Fluvial Hydrodynamics: Hydrodynamic and Sediment Transport Phenomena*. Berlin: Springer.

Dey, S. & Raikar, R.V. (2007) Characteristics of horseshoe vortex in developing scour holes at piers. *Journal of Hydraulic Engineering*, 133(4), 399–413. https://doi.org/10.1061/(ASCE)0733-9429(2007)133:4(399)

Diab, R., Link, O. & Zanke, U. (2010) Geometry of developing and equilibrium scour holes at bridge piers in gravel. *Canadian Journal of Civil Engineering*, 37(4), 544–552. https://doi.org/10.1139/L09-176

Escauriaza, C. & Sotiropoulos, F. (2011a) Initial stages of erosion and bed form development in a turbulent flow around a cylindrical pier. *Journal of Geophysical Research*, 116(F3), 671.

Escauriaza, C. & Sotiropoulos, F. (2011b) Reynolds number effects on the coherent dynamics of the turbulent horseshoe vortex system. *Flow, Turbulence and Combustion*, 86(2), 231–262. https://doi.org/10.1007/s10494-010-9315-y

Euler, T. & Herget, J. (2012) Controls on local scour and deposition induced by obstacles in fluvial environments. *Catena*, 91, 35–46. https://doi.org/10.1016/j.catena.2010.11.002

Euler, T., Herget, J., Schlömer, O. & Benito, G. (2017) Hydromorphological processes at submerged solitary boulder obstacles in streams. *Catena*, 157, 250–267. https://doi.org/10.1016/j.catena.2017.05.028

Fisher, A.C. & Klingman, P.C. (1984) Local scour at fish rocks. In: Schreiber, D.L. (Ed.) *Water for Resource Development: Proceedings of the Conference*. New York: ASCE, pp. 286–290.

Gazi, A.H. & Afzal, M.S. (2020) A review on hydrodynamics of horseshoe vortex at a vertical cylinder mounted on a flat bed and its implication to scour at a cylinder. *Acta Geophysica*, 68(3), 861–875. https://doi.org/10.1007/s11600-020-00439-8

Ghilardi, T., Franca, M.J. & Schleiss, A.J. (2014) Period and amplitude of bedload pulses in a macro-rough channel. *Geomorphology*, 221, 95–103. https://doi.org/10.1016/j.geomorph.2014.06.006

Grams, P.E., Buscombe, D., Topping, D.J., Kaplinski, M. & Hazel, J.E. (2019) How many measurements are required to construct an accurate sand budget in a large river? Insights from analyses of signal and noise. *Earth Surface Processes and Landforms*, 44(1), 160–178. https://doi.org/10.1002/esp.4489

Grams, P.E., Topping, D.J., Schmidt, J.C., Hazel, J.E. & Kaplinski, M. (2013) Linking morphodynamic response with sediment mass balance on the Colorado River in marble canyon: Issues of scale, geomorphic setting, and sampling design. *Journal of Geophysical Research - Earth Surface*, 118(2), 361–381. https://doi.org/10.1002/jgrf.20050

Hager, W.H. & Hutter, K. (1984) On pseudo-uniform flow in open channel hydraulics. *Acta Mechanica*, 53(3–4), 183–200. https://doi.org/10.1007/BF01177950

Hargitai, H. (2014) Obstacle dunes and obstacle marks. In: Hargitai, H. & Kereszturi, Á. (Eds.) *Encyclopedia of Planetary Landforms*. Heidelberg: Springer, pp. 1–5.

Hazel, J.E., Topping, D.J., Schmidt, J.C. & Kaplinski, M. (2006) Influence of a dam on fine-sediment storage in a canyon river. *Journal of Geophysical Research*, 111(F1), 919.

Herget, J. (2005) *Reconstruction of Pleistocene ice-dammed lake outburst floods in the Altai Mountains, Siberia*, Special Paper 366. Boulder, CO: Geological Society of America.

Herget, J., Euler, T., Roggenkamp, T. & Zemke, J. (2013) Obstacle marks as palaeohydraulic indicators of Pleistocene megafloods. *Hydrology Research*, 44(2), 300–317. https://doi.org/10.2166/nh.2012.155

Hodge, R.A., Hoey, T.B. & Sklar, L.S. (2011) Bed load transport in bedrock rivers: The role of sediment cover in grain entrainment, translation, and deposition. *Journal of Geophysical Research*, 116(F4), 21.

Hoffmans, G.J.C.M. (1993) *A Hydraulic and Morphologic Criterion for Upstream Slopes in Local-Scour Hole: Report W-DWW-93.255*. Delft: TUDelft.

Hoffmans, G.J.C.M. & Verheij, H.J. (1997) *Scour Manual*. Rotterdam: CRC Press.

Hong, J.-H, Chiew, Y.-M., Yeh, P.-H. & Chan, H.-C. (2017) Evolution of local pier-scour depth with dune migration in subcritical flow conditions. *Journal of Hydraulic Engineering*, 143(4), 4016098. https://doi.org/10.1061/(ASCE)HY.1943-7900.0001261

Hunt, J.C.R., Abell, C.J., Peterka, J.A. & Woo, H. (1978) Kinematical studies of the flows around free or surface-mounted obstacles; applying topology to flow visualization. *Journal of Fluid Mechanics*, 86(1), 179–200. https://doi.org/10.1017/S0022112078001068

Johnson, P.A., Clopper, P.E., Zevenbergen, L.W. & Lagasse, P.F. (2015) Quantifying uncertainty and reliability in bridge scour estimations. *Journal of Hydraulic Engineering*, 141(7), 4015013. https://doi.org/10.1061/(ASCE)HY.1943-7900.0001017

Jomaa, S, Barry, D.A., Heng, B.C.P., Brovelli, A., Sander, G.C. & Parlange, J.-Y. (2012) Influence of rock fragment coverage on soil erosion and hydrological response: Laboratory flume experiments and modeling. *Water Resources Research*, 48(5). https://doi.org/10.1029/2011WR011255

Judd, H.E, Peterson, D.E. (1969) *Hydraulics of Large Bed Element Channels: Report PRWG 17–6*. Logan, UT: Utah Water Research Laboratory.

Kaplinski, M., Hazel, J.E. Jr, Grams, P.E., Kohl, K., Buscombe, D.D. & Tusso, R.B. (2017a) *Channel Mapping River Miles 29–62 of the Colorado River in Grand Canyon National Park, Arizona, May 2009*: U.S. Geological Survey Open-File Report 2017–1030. Reston, VA: USGS.

Kaplinski, M., Hazel Jr J.E., Grams, P.E., Kohl, K., Buscombe, D.D. & Tusso, R.B. (2017b) *Channel Mapping of the Colorado River in Grand Canyon National Park, Arizona, May 2009, River Miles 29 to 62—Data*: U.S. Geological Survey data release. Reston, VA: USGS. https://doi.org/10.5066/F7930RCG

Karcz, I. (1968) Fluviatile obstacle marks from the wadis of the Negev (southern Israel). *SEPM Journal of Sedimentary Research*, 38(4), 1000–1012.

Karcz, I. (1972) Sedimentary structures formed by flash floods in southern Israel. *Sedimentary Geology*, 7(3), 161–182. https://doi.org/10.1016/0037-0738(72)90001-2

Kirkil, G. & Constantinescu, G. (2010) Flow and turbulence structure around an in-stream rectangular cylinder with scour hole. *Water Resources Research*, 46(11), W11549.

Kirkil, G. & Constantinescu, G. (2015) Effects of cylinder Reynolds number on the turbulent horseshoe vortex system and near wake of a surface-mounted circular cylinder. *Physics of Fluids*, 27(7), 75102. https://doi.org/10.1063/1.4923063

Kirkil, G., Constantinescu, S.G. & Ettema, R. (2008) Coherent structures in the flow field around a circular cylinder with scour hole. *Journal of Hydraulic Engineering*, 134(5), 572–587. https://doi.org/10.1061/(ASCE)0733-9429(2008)134:5(572)

Kothyari, U.C., Garde, R.C.J. & Ranga Raju, K.G. (1992) Temporal variation of scour around circular bridge piers. *Journal of Hydraulic Engineering*, 118(8), 1091–1106. https://doi.org/10.1061/(ASCE)0733-9429(1992)118:8(1091)

Laronne, J.B., Garcia, C. & Reid, I. (2001) Mobility of patch sediment in gravel bed streams: Patch character and its implications for bedload. In: Mosley, M.P. (Ed.) *Gravel-Bed Rivers*. Wellington: New Zealand Hydrological Society, pp. 249–289.

Launay, G., Mignot, E., Riviere, N. & Perkins, R. (2017) An experimental investigation of the laminar horseshoe vortex around an emerging obstacle. *Journal of Fluid Mechanics*, 830, 257–299. https://doi.org/10.1017/jfm.2017.582

Lawless, M. & Robert, A. (2001) Three-dimensional flow structure around small-scale bedforms in a simulated gravel-bed environment. *Earth Surface Processes and Landforms*, 26(5), 507–522. https://doi.org/10.1002/esp.195

Leary, K.C.P. & Buscombe, D. (2020) Estimating sand bed load in rivers by tracking dunes: A comparison of methods based on bed elevation time series. *Earth Surface Dynamics*, 8(1), 161–172. https://doi.org/10.5194/esurf-8-161-2020

Lee, S.O. & Sturm, T.W. (2009) Effect of sediment size scaling on physical modeling of bridge pier scour. *Journal of Hydraulic Engineering*, 135(10), 793–802. https://doi.org/10.1061/(ASCE)HY.1943-7900.0000091

Li, J., Qi, M., Fuhrman, D.R. & Chen, Q. (2018) Influence of turbulent horseshoe vortex and associated bed shear stress on sediment transport in front of a cylinder. *Experimental Thermal and Fluid Science*, 97, 444–457. https://doi.org/10.1016/j.expthermflusci.2018.05.008

Link, O., Mignot, E., Roux, S., Camenen, B., Escauriaza, C., Chauchat, J. *et al.* (2019) Scour at bridge foundations in supercritical flows: An analysis of knowledge gaps. *Water*, 11(8), 1656. https://doi.org/10.3390/w11081656

Link, O., Pfleger, F. & Zanke, U. (2008) Characteristics of developing scour-holes at a sand-embedded cylinder. *International Journal of Sediment Research*, 23(3), 258–266. https://doi.org/10.1016/S1001-6279(08)60023-2

Lisle, T.E. (1981) Roughness elements, a key resource to improve anadromous fish habitat. In: Hassler, T.J. (Ed.) *Proceedings of a Symposium on Propagation, Enhancement, and Rehabilitation of Anadromous Salmonid Populations and Habitat in the Pacific Northwest*. Arcata: Humboldt State University, pp. 93–98.

Lu, J.-Y, Shi, Z.-Z., Hong, J.-H., Lee, J.-J. & Raikar, R.V. (2011) Temporal variation of scour depth at nonuniform cylindrical piers. *Journal of Hydraulic Engineering*, 137(1), 45–56. https://doi.org/10.1061/(ASCE)HY.1943-7900.0000272

Melville, B.W. & Chiew, Y.-M. (1999) Time scale for local scour at bridge piers. *Journal of Hydraulic Engineering*, 125(1), 59–65. https://doi.org/10.1061/(ASCE)0733-9429(1999)125:1(59)

Melville, B.W. & Coleman, S.E. (2000) *Bridge Scour*. Highlands Ranch, CO: Water Resources Publications.

Mia, M.F. & Nago, H. (2003) Design method of time-dependent local scour at circular bridge pier. *Journal of Hydraulic Engineering*, 129(6), 420–427. https://doi.org/10.1061/(ASCE)0733-9429(2003)129:6(420)

Mohammadpour, R., Ab. Ghani, A., Zakaria, N.A. & Mohammed Ali, T.A. (2017) Predicting scour at river bridge abutments over time. *Proceedings of the Institution of Civil Engineers: Water Management*, 170(1), 15–30. https://doi.org/10.1680/jwama.14.00136

Mueller, D.S. & Wagner, C.R. (2005) *Field Observations and Evaluations of Streambed Scour at Bridges*: Publication no. FHWA-RD-03-052. Washington, D.C.: U.S. Department of Transportation.

Muzzammil, M. & Gangadhariah, T. (2003) The mean characteristics of horseshoe vortex at a cylindrical pier. *Journal of Hydraulic Research*, 41(3), 285–297. https://doi.org/10.1080/00221680309499973

Nakagawa, H. & Nezu, I. (1993) *Turbulence in Open Channel Flows*. Rotterdam: CRC Press.

Oliveto, G. & Hager, W.H. (2002) Temporal evolution of clear-water pier and abutment scour. *Journal of Hydraulic Engineering*, 128(9), 811–820. https://doi.org/10.1061/(ASCE)0733-9429(2002)128:9(811)

Oliveto, G. & Hager, W.H. (2005) Further results to time-dependent local scour at bridge elements. *Journal of Hydraulic Engineering*, 131(2), 97–105. https://doi.org/10.1061/(ASCE)0733-9429(2005)131:2(97)

Oliveto, G. & Hager, W.H. (2014) Morphological evolution of dune-like bed forms generated by bridge scour. *Journal of Hydraulic Engineering*, 140(5), 6014009. https://doi.org/10.1061/(ASCE)HY.1943-7900.0000853

Pagliara, S. & Palermo, M. (2008) Scour control and surface sediment distribution downstream of block ramps. *Journal of Hydraulic Research*, 46(3), 334–343. https://doi.org/10.3826/jhr.2008.3208

Pagliara, S. & Palermo, M. (2018) Equilibrium scour morphology downstream of rock sills under unsteady flow conditions. *E3S Web of Conferences*, 40, 3004.

Paik, J., Escauriaza, C. & Sotiropoulos, F. (2007) On the bimodal dynamics of the turbulent horseshoe vortex system in a wing-body junction. *Physics of Fluids*, 19(4), 45107. https://doi.org/10.1063/1.2716813

Papanicolaou, A.N., Dermisis, D.C. & Elhakeem, M. (2011) Investigating the role of clasts on the movement of sand in gravel bed rivers. *Journal of Hydraulic Engineering*, 137(9), 871–883. https://doi.org/10.1061/(ASCE)HY.1943-7900.0000381

Papanicolaou, A.N., Kramer, C.M., Tsakiris, A.G., Stoesser, T., Bomminayuni, S. & Chen, Z. (2012) Effects of a fully submerged boulder within a boulder array on the mean and turbulent flow fields: Implications to bedload transport. *Acta Geophysica*, 60(6), 1502–1546. https://doi.org/10.2478/s11600-012-0044-6

Papanicolaou, A.N. & Tsakiris, A.G. (2017) Boulder effects on turbulence and bedload transport. In: Tsutsumi, D. & Laronne, J.B. (Eds.) *Gravel-bed Rivers: Processes and Disasters*. Chichester: Wiley, pp. 33–72.

Papanicolaou, A.N., Tsakiris, A.G. & Kramer, C.M. (2010) Effects of relative submergence on flow and sediment patterns around clasts. In: Dittrich, A. (Ed.) *River Flow 2010: Proceedings of the 5th International Conference on Fluvial Hydraulics, Braunschweig, Germany, 8–10 June 2010*. Karlsruhe: Bundesanst. für Wasserbau, pp. 793–799.

Papanicolaou, A.N., Tsakiris, A.G., Wyssmann, M.A. & Kramer, C.M. (2018) Boulder array effects on bedload pulses and depositional patches. *Journal of Geophysical Research - Earth Surface*, 123(11), 2925–2953. https://doi.org/10.1029/2018JF004753

Pattenden, R.J., Turnock, S.R. & Zhang, X. (2005) Measurements of the flow over a low-aspect-ratio cylinder mounted on a ground plane. *Experiments in Fluids*, 39(1), 10–21. https://doi.org/10.1007/s00348-005-0949-9

Pizarro, A., Manfreda, S. & Tubaldi, E. (2020) The science behind scour at bridge foundations: A review. *Water*, 12(2), 374. https://doi.org/10.3390/w12020374

Pizarro, A. & Tubaldi, E. (2019) Quantification of modelling uncertainties in bridge scour risk assessment under multiple flood events. *Geosciences*, 9(10), 445. https://doi.org/10.3390/geosciences9100445

Poesen, J.W., Torri, D. & Bunte, K. (1994) Effects of rock fragments on soil erosion by water at different spatial scales: A review. *Catena*, 23(1–2), 141–166. https://doi.org/10.1016/0341-8162(94)90058-2

Poggi, D. & Kudryavtseva, N.O. (2019) Non-intrusive underwater measurement of local scour around a bridge pier. *Water*, 11(10), 2063. https://doi.org/10.3390/w11102063

Radice, A., Porta, G. & Franzetti, S. (2009) Analysis of the time-averaged properties of sediment motion in a local scour process. *Water Resources Research*, 45(3), 1069.

Radice, A. & Tran, C.K. (2012) Study of sediment motion in scour hole of a circular pier. *Journal of Hydraulic Research*, 50(1), 44–51. https://doi.org/10.1080/00221686.2011.641764

Rennie, S.E., Brandt, A. & Friedrichs, C.T. (2017) Initiation of motion and scour burial of objects underwater. *Ocean Engineering*, 131, 282–294. https://doi.org/10.1016/j.oceaneng.2016.12.029

Richardson, P.D. (1968) The generation of scour marks near obstacles. *SEPM Journal of Sedimentary Research*, 38(4), 965–970.

Rogers, A., Manes, C. & Tsuzaki, T. (2020) Measuring the geometry of a developing scour hole in clear-water conditions using underwater sonar scanning. *International Journal of Sediment Research*, 35(1), 105–114. https://doi.org/10.1016/j.ijsrc.2019.07.005

Sarkar, K., Chakraborty, C. & Mazumder, B.S. (2015) Spacetime dynamics of bed forms due to turbulence around submerged bridge piers. *Stochastic Environmental Research and Risk Assessment*, 29(3), 995–1017. https://doi.org/10.1007/s00477-014-0961-9

Schalko, I., Lageder, C., Schmocker, L., Weitbrecht, V. & Boes, R.M. (2019) Laboratory flume experiments on the formation of spanwise large wood accumulations part II: Effect on local scour. *Water Resources Research*, 55(6), 4871–4885. https://doi.org/10.1029/2019WR024789

Schlömer, O. (2020) Morphometric relation of obstacle marks at boulder-like obstructions in time. In: Uijttewal, W., Blom, A. & Franca, M. (Eds.) *River Flow 2020: Proceedings of the International Conference on Fluvial Hydraulics, Delft, Netherlands, 7–10 July*. Rotterdam: CRC Press/Balkema, pp. 719–727.

Schlömer, O., Herget, J. & Euler, T. (2020) Boundary condition control of fluvial obstacle mark formation – framework from a geoscientific perspective. *Earth Surface Processes and Landforms*, 45(1), 189–206. https://doi.org/10.1002/esp.4793

Shamloo, H., Rajaratnam, N. & Katopodis, C. (2001) Hydraulics of simple habitat structures. *Journal of Hydraulic Research*, 39(4), 351–366. https://doi.org/10.1080/00221680109499840

Sheppard, D.M. & Melville, B., Demir, H. (2014) Evaluation of existing equations for local scour at bridge piers. *Journal of Hydraulic Engineering*, 140(1), 14–23. https://doi.org/10.1061/(ASCE)HY.1943-7900.0000800

Simarro, G., Fael, C.M.S & Cardoso, A.H. (2011) Estimating equilibrium scour depth at cylindrical piers in experimental studies. *Journal of Hydraulic Engineering*, 137(9), 1089–1093. https://doi.org/10.1061/(ASCE)HY.1943-7900.0000410

Sonia Devi, Y. & Barbhuiya, A.K. (2017) Bridge pier scour in cohesive soil: A review. *Sādhanā*, 42(10), 1803–1819. https://doi.org/10.1007/s12046-017-0698-5

Storm, K.B. & Papanicolaou, A.N. (2007) Morphological characterization of cluster microforms. *Sedimentology*, 55(1), 137–153.

Sumner, D. (2013) Flow above the free end of a surface-mounted finite-height circular cylinder: A review. *Journal of Fluids and Structures*, 43, 41–63. https://doi.org/10.1016/j.jfluidstructs.2013.08.007

Sutherland, J. & Soulsby, R. (2011) Sediment dynamics. In: Frostick, L.E., McLelland, S.J. & Mercer, T.G. (Eds.) *Users Guide to Physical Modelling and Experimentation: Experience of the HYDRALAB Network*. Hoboken, NJ: CRC Press, pp. 67–125.

Thompson, D.M. (2008) The influence of lee sediment behind large bed elements on bedload transport rates in supply-limited channels. *Geomorphology*, 99(1–4), 420–432. https://doi.org/10.1016/j.geomorph.2007.12.004

Tregnaghi, M., Marion, A. & Gaudio, R. (2007) Affinity and similarity of local scour holes at bed sills. *Water Resources Research*, 43(11), W11417.

Tubaldi, E., Macorini, L., Izzuddin, B.A., Manes, C. & Laio, F. (2017) A framework for probabilistic assessment of clear-water scour around bridge piers. *Structural Safety*, 69, 11–22. https://doi.org/10.1016/j.strusafe.2017.07.001

Unger, J. & Hager, W.H. (2007) Down-flow and horseshoe vortex characteristics of sediment embedded bridge piers. *Experiments in Fluids*, 42(1), 1–19.

USGS National Bridge Scour Database. (2020) http://water.usgs.gov/osw/techniques/bs/BSDMS/BSDMS_1.html [Accessed 10th September 2020].

Williams, P., Balachandar, R. & Bolisetti, T. (2019) Examination of blockage effects on the progression of local scour around a circular cylinder. *Water*, 11(12), 2631. https://doi.org/10.3390/w11122631

SUPPORTING INFORMATION

Additional supporting information may be found online in the Supporting Information section at the end of this article.

How to cite this article: Schlömer O, Grams PE, Buscombe D, Herget J. Geometry of obstacle marks at instream boulders—integration of laboratory investigations and field observations. *Earth Surf. Process. Landforms*. 2021;46:659–679. https://doi.org/10.1002/esp.5055